Proteomics Identification of Annexin A2 as a Key Mediator in the Metastasis and Proangiogenesis of Endometrial Cells in Human Adenomyosis*

Shengtao Zhou, Tao Yi, Rui Liu, Ce Bian, Xiaorong Qi, Xiang He, Kui Wang, Jingyi Li, Xia Zhao‡, Canhua Huang§, and Yuquan Wei

Adenomyosis is a common estrogen-dependent disorder of females characterized by a downward extension of the endometrium into the uterine myometrium and neovascularization in ectopic lesions. It accounts for chronic pelvic pain, dysmenorrhea, menorrhagia, and infertility in 8.8–61.5% women worldwide. However, the molecular mechanisms for adenomyosis development remain poorly elucidated. Here, we utilized a two-dimensional polyacrylamide gel electrophoresis/MS-based proteomics analysis to compare and identify differentially expressed proteins in matched ectopic and eutopic endometrium of adenomyosis patients. A total of 93 significantly altered proteins were identified by tandem MS analysis. Further cluster analysis revealed a group of estrogen-responsive proteins as dysregulated in adenomyosis, among which annexin A2, a member of annexin family proteins, was found up-regulated most significantly in the ectopic endometrium of adenomyosis compared with its eutopic counterpart. Overexpression of ANXA2 was validated in ectopic lesions of human adenomyosis and was found to be tightly correlated with markers of epithelial to mesenchymal transition and dysmenorrhea severity of adenomyosis patients. Functional analysis demonstrated that estrogen could remarkably up-regulate ANXA2 and induce epithelial to mesenchymal transition in an *in vitro* adenomyosis model. Enforced expression of ANXA2 could mediate phenotypic mesenchymal-like cellular changes, with structural and functional alterations in a β-catenin/T-cell factor (Tcf) signaling-associated manner, which could be reversed by inhibition of ANXA2 expression. We also proved that enforced expression of ANXA2 enhanced the proangiogenic capacity of adenomyotic endometrial cells through HIF-1α/VEGF-A pathway. *In vivo*, we demonstrated that ANXA2 inhibition abrogated endometrial tissue growth, metastasis, and angiogenesis in an adenomyosis nude mice model and significantly alleviated hyperalgesia. Taken together, our data unraveled a dual role for ANXA2 in the pathogenesis of human adenomyosis through conferring endometrial cells both metastatic potential and proangiogenic capacity, which could serve as a potential therapeutic target for the treatment of adenomyosis patients. ***Molecular & Cellular Proteomics 11: 10.1074/mcp.M112.017988, 1–24, 2012.***

Adenomyosis is one of the most common gynecological ailments that can arise as diffuse and/or focal, tumor-like growth, whose defining feature is the aberrant growth and invasion of endometrium-like tissue into the myometrium and myometrial hypertrophy/hyperplasia, which is supported by neovasculature in ectopic lesions. It preferentially inflicts multiparous women in their reproductive or perimenopausal years, and its prevalence worldwide has been reported to range from 8.8 to 61.5% in women at the time of hysterectomy (1, 2). Approximately two-thirds of adenomyosis patients suffer from dysmenorrhea (15–30%), menorrhagia (40–50%), metrorrhagia (10–12%), or even early pregnancy stage miscarriages, thereby greatly compromising their physical, mental, and social well being. Although a growing body of evidence recently linked the pathogenesis of adenomyosis to a remarkable disorder of estrogen metabolism, the molecular mechanisms of this disease still remain largely unelucidated.

Epithelial to mesenchymal transition (EMT)[1] is a process characterized by a loss of polarity of epithelial cells and transition to a mesenchymal phenotype (3). It has been reported both under physiological situations like wound healing (4) and

From the Department of Gynecology and Obstetrics, Key Laboratory of Obstetrics & Gynecologic and Pediatric Diseases and Birth Defects of Ministry of Education, West China Second Hospital and the State Key Laboratory of Biotherapy, West China Hospital, Sichuan University, Chengdu 610041, China

Received February 11, 2012, and in revised form, March 30, 2012
Published, MCP Papers in Press, April 9, 2012, DOI 10.1074/mcp.M112.017988

[1] The abbreviations used are: EMT, epithelial to mesenchymal transition; 2-DE, two-dimensional polyacrylamide gel electrophoresis; ANXA2, annexin A2; E2, estrogen; TAM, Tamoxifen; Tcf, T-cell factor; VEGF-A, Vascular endothelial growth factor A; siRNA, small interfering RNA; shRNA, short hairpin RNA; MTT, 3-(4,5-dimethylthiazol-2-yl)-2,5-diphenyltetrazolium bromide; TUNEL, terminal deoxynucleotidyltransferase dUTP nick-end labeling; HUVEC, human umbilical vein endothelial cell; NC, negative control; HIF, hypoxia-inducible factor; DAPI, 4′,6′-diamino-2-phenylindole; NS, normal saline.

during development as well as in malignant cells undergoing invasion and metastasis, which could be initiated through a variety of stimuli, including hormonal turbulence, genetic mutation, or hypoxia (5). The molecular events of EMT include down-regulation of epithelial markers (*e.g.*, E-cadherin) and overexpression of mesenchymal markers (*e.g.*, fibronectin and vimentin), which involves activation of a number of transcription factors, including Snail, Slug, Twist, Zeb1, and SIP1. Existing evidences have showed invasive behavior and cytoskeletal rearrangement of endometrial epithelial cells during ectopic implantation concomitant with reduced expression of E-cadherin (6) and up-regulation of vimentin expression (7) in endometriotic lesions compared with normal uterine endometrium. These data implicate a possible role of EMT in adenomyosis development. On the other hand, blood vessel formation through angiogenesis involves the induction of new sprouts, coordinated and directed endothelial cell migration, proliferation, sprout fusion (anastomosis), and lumen formation (8), which is tightly regulated by the balance of various proangiogenic stimulators and angiogenesis inhibitors (9). Previous studies documented that the endometrium in adenomyotic foci is highly vascularized with dilated microvessels (10). Thus, we hypothesize that after migration to an ectopic location, endometrial cells initiate a series of proangiogenic events responsible for neovascularization to support their ectopic growth.

Two-dimensional polyacrylamide gel electrophoresis (2-DE)-based proteomics has been proved a powerful tool to simultaneously analyze the expression patterns of proteins in tissue samples and has been successfully applied in the investigation of a variety of diseases (11, 12). Here, we utilized a 2-DE/MS-based proteomics approach to compare differentially expressed proteins between matched ectopic and eutopic endometrium of human adenomyosis and identified annexin A2 (ANXA2) as one of the most significantly altered estrogen-responsive proteins in ectopic endometrium of adenomyosis compared with its eutopic counterpart. Further functional analysis unraveled a dual role of ANXA2 in the pathogenesis of human adenomyosis through conferring endometrial cells metastatic potential and proangiogenic capacity.

EXPERIMENTAL PROCEDURES

Clinical Specimens—Freshly resected matched ectopic and eutopic endometrial tissues of 28 adenomyosis or adenomyoma patients who underwent hysterectomy were collected at the Gynecological Department of West China Second Hospital of Sichuan University (Chengdu, China) from 2009 to 2010. Each donor was taking no medications, and none received hormone therapy prior to surgery. Tissue samples were immediately snap frozen in liquid nitrogen and stored at −80 °C. A subsample encompassing eight pairs of samples was randomly selected for 2-DE analysis as described previously (11). All of these samples were obtained by experienced gynecologists and gynecological surgeons and examined by experienced pathologists who confirmed the diagnosis of disease samples in which there was ingrowth of endometrium >2.5 mm below the endometrial-myometrial interface. This study was approved by the Institutional Ethics Committee of Sichuan University. Informed consents were obtained from all patients prior to analysis.

2-DE Analysis—2-DE proteomics analysis was performed as described previously (12). Briefly, 100 mg of tissue samples were ground into fine powder in liquid nitrogen and lysed in lysis buffer (8 M urea, 2 M thiourea, 4% CHAPS; Bio-Rad) containing protease inhibitor mixture 8340 (Sigma-Aldrich). The samples were subsequently kept on ice, ultrasonicated for 10 cycles each consisting of a 10-s sonication followed by a 30-s break, and finally held for 30 min on ice with periodic Vortex mixing. After centrifugation at 14,000 rpm for 45 min at 4 °C, the supernatant was precipitated with cold acetone at −20 °C for 1 h and dissolved with rehydration buffer (8 M urea, 2 M thiourea, 4% CHAPS, 100 mM DTT, 2% ampholyte). The protein concentration of the supernatants was quantified using the DC protein assay kit (Bio-Rad). The protein extracts were either applied immediately to IEF or stored at −80 °C in aliquots prior to analysis. ReadyStrip™ IPG strips were passively rehydrated using 300 μl (equal to 2.5 mg of protein) of each paired preparation (17 cm, pH 3–10 nonlinear; Bio-Rad). After 16 h of rehydration, the strips were transferred to a PROTEAN IEF cell (Bio-Rad). IEF was performed as follows: 250 V for 30 min, linear; 1000 V for 1 h, rapid; linear ramping to 10,000 V for 5 h; and finally 10,000 V for 6 h. Once IEF was completed, the strips were equilibrated in equilibration buffer (25 mM Tris-HCl, pH 8.8, 6 M urea, 20% glycerol, 2% SDS, 130 mM DTT) for 15 min and washed with 50 mM Tris-HCl, pH 8.8, 6 M urea, 20% glycerol, 2% SDS, 200 mM iodoacetamide for another 15 min. The second dimension was performed using 12% SDS-PAGE at 30 mA constant current per gel. The protein spots in gels were visualized by Coomassie Brilliant Blue G-250 staining (Merck). For 2-DE analysis, each of the paired samples was run in triplicate to ensure the consistency of the data.

Image Analysis—The images were scanned with a Bio-Rad GS-800 scanner (400–750 nm), and the differentially expressed proteins were identified using the PDQuest 2-DE analysis software (Bio-Rad). Two independent observers then visually confirmed differential expression. The quantity of each spot in a gel was normalized as a percentage of the total quantity in the map according to its optical density value. Only those spots that changed consistently (recurred for more than three times) and significantly (more than 2-fold) were selected for further MS/MS analysis.

Tryptic In-gel Digestion—In-gel digestion of proteins was carried out using mass spectrometry grade trypsin gold (Promega, Madison, WI) according to the manufacturer's protocol. Briefly, spots were excised (1–2-mm in diameter) using a razor blade and destained twice with 100 mM NH_4HCO_3, 50% ACN at 37 °C for 45 min in each treatment. After dehydration with 100% ACN and drying, the gels were preincubated in 10–20 μl of trypsin solution (10 ng/μl) for 1 h. Subsequently adequate digestion buffer (40 mM NH_4HCO_3, 10% ACN) was added to cover the gels, which were incubated overnight at 37 °C (12–14 h). Tryptic digests were extracted using Milli-Q water followed by double extraction with 50% ACN, 5% TFA for 1 h each time. The combined extracts were dried in a SpeedVac concentrator (Thermo Scientific) at 4 °C. The samples were then subjected to mass spectrometry.

ESI-Q-TOF—Mass spectra were acquired using a Q-TOF mass spectrometer (Micromass, Manchester, UK) fitted with an ESI source (Waters). Tryptic digests were dissolved in 18 μl of 50% ACN. MS/MS was performed in a data-dependent mode in which the top 10 most abundant ions for each MS scan were selected for MS/MS analysis. Trypsin autolysis products and keratin-derived precursor ions were automatically excluded. The MS/MS data were acquired and processed using MassLynx V4.1 software (Micromass), and Mascot from Matrix Science in June 2009 was used to search the database. Database searches were carried out using the following parameters:

database, Swiss-Prot 57.3/NCBI (468,851 sequences); taxonomy, *Homo sapiens* (20,401 sequences); enzyme, trypsin; and an allowance of one missed cleavage. Fixed modifications of carbamidomethylation and variable modifications of oxidation/phosphorylation were allowed. The peptide and fragment mass tolerances were set at 1 and 0.2 Da, respectively. The data format was selected as Micromass PKL, and the instrument was selected as ESI-Q-TOF. Proteins with probability-based MOWSE scores exceeding their threshold ($p < 0.05$) were considered to be positively identified. If proteins were identified by a single peptide, the spectrum was validated manually. For a protein to be accepted, the assignment had to be based on four or more y- or b-series ions. To eliminate the redundancy of proteins appearing in the database under different names or accession numbers, the one protein member with the highest MASCOT score and belonging to the species *H. sapiens* was further selected from the relevant multiple member protein family.

Bioinformatics Analysis—For bioinformatics analysis, the open source web-based tool STRING was utilized to analyze the protein-protein interaction networks as described previously (13). STRING is a pool of established and predicted protein interactions that integrates biomolecular interaction networks with high throughput expression results and other molecular states into a unified conceptual framework, for a better annotation of molecular components and interactions.

Cell Lines, Drug Treatment, and Antibodies—The estrogen receptor-positive ISK (Ishikawa) cell line (human Asian endometrial adenocarcinoma, European Collection of Cell Cultures, No. 99040201) was cultured in RPMI 1640 medium (Invitrogen) supplemented with 10% fetal bovine serum. Human umbilical vein endothelial cells (HUVEC) were isolated from human umbilical cord veins using a standard procedure as previously described (14) and grown in EBM-2 medium with SingleQuots™ (Lonza, Walkersville, MD). HUVEC at passages 3–8 were used for all experiments.

At 80% confluence, ISK cells were placed in phenol red-free RPMI 1640 medium containing 10% fetal bovine serum for 48 h prior to drug treatment to remove endogenous steroids. The cells were treated with E2 (10 μM) (Sigma-Aldrich), DMSO (solvent for E2 and tamoxifen), tamoxifen (0.5 μM) (Sigma-Aldrich), E2 plus tamoxifen, or LiCl (10 mM) (Sigma-Aldrich) for 24 h. Antibodies used in this study included: rabbit anti-annexin A2, -E-cadherin, -vimentin, -slug, -HIF-1α, -VEGF-A, -β-actin antibodies purchased from Santa Cruz Biotechnology and mouse anti-CD-31 antibody purchased from Boster.

Data Set Analysis—For microarray analyses of the expression of ANXA2 and its correlation with EMT markers, three publicly available data sets were used as summarized in Table IV. The first, published by Eyster *et al.* (24), compared paired eutopic and ectopic endometrium of endometriosis patients. The data were obtained from the NCBI Gene Expression Omnibus (GSE5108). The second, published by Burney *et al.* (26), analyzed endometrial biopsies obtained from women both with normal endometrial pathologies and no history of endometriosis and from women with laporoscopy-proven moderate to severe stage endometriosis. The data were obtained from the NCBI Gene Expression Omnibus (GSE6364). The third data set, published by Hever *et al.* (25), compared paired endometriosis and normal endometrium. The data were obtained from the NCBI Gene Expression Omnibus (GSE7305).

Semiquantitative RT-PCR—Total RNAs were isolated using TRIzol reagent (Invitrogen) according to the manufacturer's instructions. First strand cDNA was reversely transcribed from 1 μg of total RNA in a final volume of 20 μl using RTase and random hexamers from ExScript reagent kit (TAKARA, Dalian, China) according to the manufacturer's instructions. The primer sequences and annealing temperature for selected genes were listed in Table V, and PCR was performed as described previously (12).

TABLE I
Clinicopathologic parameters of all patients

Clinicopathologic features	*n* (%)
Mean age (range)	43.2 ± 6.1 (31–50)[a]
Sampling time during menstrual cycle	
Proliferative phase	36 (55.4%)
Secretory phase	29 (44.6%)
Pregnancy/parity	
Multipregnancy/multiparity	41 (63.1%)
Monopregnancy/monoparity	24 (36.9%)
Histology	
Adenomyosis	48 (73.8%)
Adenomyoma	17 (26.2%)
Total	65 (100%)

[a] Mean age (range) in years.

Immunoblotting and ELISA—For immunoblotting, the whole cell lysates were prepared as described previously (14). Proteins from conditioned medium samples were precipitated by mixing 1 ml:5 ml with methanol and incubating for 1 h at −80 °C, pelleted, dried, and then subjected to further immunoblotting. The signals were quantified by QuantityOne software (Bio-Rad) and defined as the ratio of target protein to β-actin. ELISA was used to measure VEGF concentration in conditioned medium as described elsewhere (15).

Immunohistochemistry—Paraffin-embedded matched eutopic and ectopic endometrial specimens were obtained from 65 patients who underwent surgical resections from 2009 to 2010, among which 36 cases were in the proliferative phase and 29 cases were in the secretory phase. Detailed clinicopathologic information of the patients including age, race, pregnancy/parity status, sampling time during menstrual cycle, and histology was summarized in Table I. Immunohistochemistry was performed using the primary antibodies including rabbit anti-ANXA2 (diluted 1:200; Santa Cruz Biotechnology), rabbit anti-E-cadherin (diluted 1:200; Santa Cruz Biotechnology), rabbit anti-vimentin (diluted 1:200; Santa Cruz Biotechnology), rabbit anti-HIF-1α (diluted 1:200; Santa Cruz Biotechnology), rabbit anti-VEGF-A (diluted 1:100; Abcam), and mouse anti-CD31 (diluted 1:400; Boster) as described previously (12). A series of 10 random images on several sections were captured, and the immunohistochemical staining was assessed by calculating the percentage of positive glandular or stromal cells of the endometrium and the immunostaining intensity using Image-Pro Plus version 6.0 (Media Cybernetics, Baltimore, MD). The staining intensities were scored as 0, 1, 2, and 3, and the mean value of staining intensities of the 10 captured images was considered as the staining score of each specimen. The slides were evaluated by two independent pathologists in a double-blinded manner. Any discrepancy between the two evaluators was resolved by re-evaluation and careful discussion until agreement was reached.

Immunofluorescent Microscopy—Immunofluorescent microscopy was carried out as described previously (14). Stained sections were viewed and photographed using a fluorescence microscope (Olympus Optical Co., Hamburg, Germany).

Plasmids, siRNA, and Transfection—siRNA oligonucleotides with specificity for ANXA2 (AAGGACAUUAUUUCGGACACA) and nontargeting control siRNA consisting of a scrambled sequence (ACACGAGAUAAUAUCGACUUG) were obtained from GenePharma (16). Based upon the shRNA design principle, oligonucleotide sequences of ANXA2 shRNA (sense, 5′-CACCGCAAGT CCCTGTACTA TTATACGAAT ATAATAGTAC AGGGACTTGC-3′; antisense, 5′-AAAAGCAAGT CCCTGTACTA TTATATTCGT ATAATAGTAC AGGGACTTGC-3′) and nontargeting NC shRNA were designed. The plasmid Pgenesil-2 containing a kanamycin resistance gene was linearized

with BamHI and HindIII, and the annealed oligonucleotide templates were ligated into a plasmid vector using T4 DNA ligase. Chemically competent DH5α *Escherichia coli* were transformed, and positive transformants were isolated by kanamycin selection and amplified using standard methods. Identification of the insert-containing plasmids was confirmed by digestion with SalI, and plasmid DNA from positive clones was extracted and sequenced for additional verification. Once the requirement had been met, a large scale preparation of plasmid DNA was extracted.

ANXA2-plasmid encoding full-length human ANXA2 was purchased from Integrated Biotech Solutions (Shanghai, China) based on the cDNA sequence of ANXA2 (GenBank™ accession number NM_004039). For ANXA2 expression, the ANXA2 plasmid and control empty vector (designated as negative control, NC) plasmid were separately transfected into ISK cells using Lipofectamine 2000 (Invitrogen) according to the manufacturer's instructions, and the stable transfectants were selected in the presence of 0.8 mg/ml G418 (Invitrogen).

Cell Proliferation Assays—Cell proliferation was evaluated using MTT assay and colony formation assay. As for MTT assay, the cells were seeded at 5×10^3 cells/well in 96-well plates and cultivated in 100 μl of culture medium. Culture wells were set up in triplicate for each treatment, and the assay was carried out as described previously (11). As for colony formation assay, 100 counted ISK cells, ISK^{NC} cells, and ISK^{ANXA2} cells were seeded in triplicate in a 6-well plate, respectively, and cultured continuously for 14 days. Subsequently, the clones were stained with Giemsa and counted under a microscope. A cluster with more than 50 cells was considered as a clone, and the clonogenic formation rate was calculated.

Anoikis Assay—Prior to anoikis challenge, the cells were transfected with either siNC or siANXA2 for 24 h to knockdown ANXA2. Then cells (5×10^5/well) were cultured on either plastic or poly-HEMA-treated 6-well tissue culture plates for 24 h at 37 °C in a 5% CO_2 atmosphere. After incubation, adherent cells were detached with 0.5% trypsin, 0.1% EDTA in PBS. Detached and suspended cells were harvested in complete RPMI 1640 medium and centrifuged at 500 $\times$ *g* for 10 min and analyzed for apoptosis by flow cytometry analysis.

TUNEL Assay—TUNEL assay was performed using the DeadEnd™ fluorometric TUNEL system according to the manufacturer's protocol (Promega, G3250). The cells were then viewed and photographed using a fluorescence microscope (Olympus Optical Co., Hamburg, Germany), and a nucleus with bright green fluorescence staining was recorded as a TUNEL-positive cell.

TOP/FOP Flash Assay—The TOP-FLASH and FOP-FLASH luciferase reporter constructs were purchased from Upstate, and the *Renilla* luciferase plasmid (pRL-CMV) was obtained from Promega. A total of 5×10^3 ISK^{NC} cells, ISK^{ANXA2} cells or ISK cells treated with LiCl were transfected with either TOP-FLASH or FOP-FLASH plus pRL-CMV. TOP-FLASH or FOP-FLASH activity was corrected for *Renilla* activity using the Dual-Luciferase kit (Promega), and the results were expressed as a ratio of corrected TOP-FLASH/FOP-FLASH. Each experiment was performed in triplicate.

Wound Healing Assay—Wounds were created in confluent cells using a pipette tip, and the cells were then rinsed with medium to remove free-floating cells and debris. Serum-free medium was then added, and culture plates were incubated at 37 °C for 2 days. Wound healing was observed at 0 and 48 h within the scrape line, and representative scrape lines for each cell line were photographed. Duplicate wells of each condition were examined for each experiment, and each experiment was carried out in triplicate.

Cell Migration, Chemotaxis, and Invasion Assay—Transwell 24-well chambers (Corning) were used for *in vitro* cell migration, HUVEC chemotaxis, and invasion assay. For ISK cell migration, ISK cells were pretreated with siRNA for 24 h. Then they were plated in the upper chamber with RPMI 1640 medium containing 0.5% fetal bovine serum, and RPMI 1640 medium containing 20% fetal bovine serum was added to the lower chamber as chemoattractant. To analyze ISK cell-conditioned medium-mediated chemotactic motility of HUVEC cells, HUVEC cells were starved for overnight prior to assays. Conditioned medium of ISK cells, ISK^{NC} cells, and ISK^{ANXA2} cells, respectively, was placed in the lower chamber. Conditioned medium containing 20 ng/ml VEGF served as positive control. The cells were seeded (1×10^5 cells in 50 ml of suspension) in the upper chamber and incubated at 37 °C in air with 5% CO_2 for 18 h. The filters were then removed, stained with crystal violet, and the cells of five fields were counted at the inverted microscope (Zeiss Axiovert). To monitor ISK cell invasion, the upper side of the filter was covered with Matrigel (Collaborative Research Inc, Boston, MA). After 24 h for the migration assay or 48 h for the invasion assay, the cells on the upper side of the filter were removed. Cells that remained adherent to the underside of the membrane were fixed and stained with crystal violet. Each experiment was performed in triplicate, and 10 contiguous fields of each sample were examined to obtain a representative number of cells that had migrated/invaded across the membrane. The results of the migration/invasion assays were normalized to the proliferation for each group.

Tube Formation Assay—250 μl of growth factor-reduced Matrigel (BD Biosciences Discovery Labware, Bedford, MA) was added per well of a 24-well plate and allowed to polymerize at 37 °C for at least 30 min. Trypsin-harvested HUVEC cells (5×10^4) suspended in 250 μl of conditioned medium of ISK cells, ISK^{NC} cells, and ISK^{ANXA2} cells, respectively, were seeded onto Matrigel. Conditioned medium containing 20 ng/ml VEGF served as a positive control. After incubation for 6 h at 37 °C, capillary-like structures within the Matrigel layer were photographed with a digital camera attached to an inverted microscope. Total branch points per field were quantified using image analysis software of Image-Pro Plus (version 6.0; Media Cybernetics, Baltimore, MD).

Alginate-encapsulated Cell Assay in Vivo—ISK cells were resuspended in a 1.5% solution of alginate (Sigma-Aldrich) and added dropwise into a solution of 250 mM $CaCl_2$; an alginate bead was formed containing 1×10^5 cells. Four beads were then implanted subcutaneously in the back of nude mice. Eight mice were then grouped and treated as aforementioned. Treatment was initiated on the same day of implanting beads. After 2 weeks, the alginate beads were photographed after being exposed surgically. The number of cells covering the alginate beads was counted.

Xenotransplantation of Human Adenomyosis Lesions in Nude Mice and shRNA Treatment—The guidelines for animal care were approved by the Institutional Animal Care and Use Committee of Sichuan University (Chengdu, Sichuan, China). Six-week-old female nude mice (BALB-c nu/nu, nonfertile, and 18–20 g each) were housed under controlled room temperature (22 $\pm$ 2 °C) and lighting (12 h light/dark cycle) contains in filtered air laminar flow cabinets and manipulated using aseptic procedures. Adenomyotic lesions were obtained during hysterectomy from five premenopausal women with adenomyosis undergoing surgery at West China Second Hospital of Sichuan University. The age range of the women spanned from 38 to 46 years with a mean age of 42 years. Patients with a history of hormone therapy within the previous 2 months were excluded. An *in vivo* adenomyosis model was surgically induced as described previously with minor modifications (17). Briefly, fresh adenomyotic tissue biopsies were washed in prewarmed phenol-red free Dulbecco's modified Eagle's medium/Ham's F-12 medium (Sigma-Aldrich) to remove residual blood before culturing. Subsequently, biopsies were dissected into small cubes (about 1×1 mm^3), and five pieces of tissue/mouse were suspended in tissue culture inserts (Millipore, Bedford MA), which were maintained for 18–24 h prior to injection into mice under serum-free conditions in Dulbecco's modified Eagle's medium/Ham's F-12

medium supplemented with 1 nmol/liter 17β-estradiol (E2; Sigma-Aldrich). The cultures were incubated at 37 °C in a humidified chamber with 5% CO_2.

The mice were anesthetized with intraperitoneal injections of chloral hydrate and were ovariectomized through bilateral paravertebral incisions, and the wound was closed with a 5–0 braided silk suture (Ethicon). Two days later, an incision was made on the ventral midline, and the mice received an intraperitoneal injection of PBS containing a suspension of five human adenomyotic tissue fragments per mouse into the ventral midline. A subcutaneous injection of 0.5 μg of 17β-estradiol was performed on days 1 and 2 to facilitate the implantation of adenomyotic nodules. The mice were next assigned randomly to one of the following groups (seven per group): (*a*) NS, 100 μl of NS; (*b*) Lipo, Lipofectamine 2000 at 62.5 μg/100 μl of NS; (*c*) Lipo + NC shRNA, negative control shRNA at 25 μg/100 μl of NS; (*d*) Lipo + ANXA2 shRNA, ANXA2 shRNA at 25 μg/100 μl of NS. Intraperitoneal treatment was initiated 5 days after inoculation. The mice received therapy every 2 days and were sacrificed at 25 days postinoculation. Intraperitoneal endometrial nodules were resected and measured immediately to assess the treatment efficacy. The volumes of the implants were calculated as follows: $TV\ (mm^3) = (L \times W^2))/2$, where L is the longest, and W is the shortest radius of the lesion in millimeters. The implanted endometrial lesions were harvested for further hematoxylin and eosin and immunohistochemistry analysis. Pathology scores were assigned as previously described (18): 0 (receded lesion with stromal fibrosis, hemosiderine, and absence of glandular structure) to 3 (active lesion with fresh blood, profuse stromal cellular infiltration, and developed glandular organization). Scoring was performed by two different pathologists unaware of the treatments each group received.

Pain Assessment and Serum CA12-5 Levels of Adenomyosis Patients—Pain assessment was performed in 40 adenomyosis patients (these 40 patients fell into those 65 patients whose endometrial tissues were further subjected to immunohistochemical analysis) as described previously (19). Briefly, questionnaires on dysmenorrhea and other clinical information were administered before surgery during the hospital stay. Pain assessment was done with a 10-point linear analog scale, with 0 representing no pain and 10 representing the worst possible pain. The serum CA12-5 levels of 30 adenomyosis patients (these 30 patients also fell into those 65 patients whose endometrial tissues were further subjected to immunohistochemical analysis) were analyzed using ELISA as described previously (15).

Hyperalgesia Evaluation in Xenotransplantation Nude Mice Model of Human Adenomyosis—To explore whether knockdown of ANXA2 could alleviate hyperalgesia in experimental nude mice model of human adenomyosis, we utilized a combined experimental procedures including hot plate test and formalin test to evaluate their response thresholds to high intensity stimuli (acute pain tests) and changes in spontaneous or evoked behavioral responses, respectively, as described previously (20, 21). As for hot plate test, a commercially available hot plate analgesia meter (RB-200; TME Technology, Chengdu, China) consisting of a metal plate with a constant temperature of 54.0 ± 0.1 °C was utilized, on which a plastic cylinder was placed. Mice (seven per group) were then grouped and treated as aforementioned. Prior to the test, the mice were brought to the testing room and allowed to acclimatize for 10 min. The latency to respond to thermal stimulus, defined as the time (in second) elapsed from the moment when the mouse was inserted inside the cylinder to the time when it licked or flicked its hind paws, jolted, or jumped off the hot plate. Each animal was tested only once in one session. The latency was calculated as the mean of two readings recorded at intervals of 24 h. As for formalin test, the mice (seven per group) were grouped and treated as aforementioned. Pain was induced by injecting 0.05 ml of 2.5% formalin subcutaneously in the subplantar of the right hindpaw of the nude mice. These nude mice were placed in separate cages for the observation. The time spent licking the injected paw was considered as indicative of pain. Nociceptive responses were measured for first 5 min (early phase) and 15–30 min (late phase) after formalin injection.

Statistical Analysis—The data are presented as the means ± S.D. of three independent experiments unless otherwise indicated. GraphPad Prism (GraphPad Software Inc., La Jolla, CA) was used for data analysis with all data assessed for normal distribution and equal variance. The correlation between ANXA2 staining scores and dysmenorrhea scores or serum CA12-5 levels was analyzed using a Pearson χ^2 test. Comparisons between two groups were performed Student's t test, and differences among multiple groups were evaluated by one-way analysis of variance. Differences were considered statistically significant at $p < 0.05$.

RESULTS

Proteomics Profiling of Differentially Expressed Proteins between Matched Ectopic and Eutopic Endometrium in Human Adenomyosis—To identify candidate proteins responsible for the pathogenesis of adenomyosis, we performed 2-DE/MS analysis between matched ectopic and eutopic endometrium of adenomyosis. Representative 2-DE maps for a subsample of eight pairs of samples, which were matched by the PD-Quest software, are shown in Fig. 1*A*. Differentially expressed proteins were defined as statistically significant ($p < 0.05$) when their intensity alterations were over 2.0-fold and at the same time recurred more than three times. By applying these criteria, we identified 93 spots as differentially expressed (Table II), among which 40 proteins were up-regulated, whereas 53 proteins were down-regulated. 18 representative proteins (9 up-regulated and 9 down-regulated in ectopic endometrial samples of adenomyosis) with the most significant alterations were boxed, enlarged in the surrounding area, and labeled with *arrows* (Fig. 1*D*). The arbitrary expression values of these 18 proteins are shown in Fig. 1*E*.

Mass Spectrum Identification of Differentially Expressed Proteins—The 93 spots with differential expression levels were further subjected to MS/MS analysis. The MS/MS data were retrieved using the search algorithm MASCOT against the ExPASy protein sequence database. The proteins were identified using such criteria as pI, molecular weight, the number of matched peptides, sequence coverage, and MOWSE scores. All of the protein information was listed in Table II. Cluster maps (Fig. 1*F*) illustrating altered expression of the 93 proteins were generated by Cluster software. These proteins fell into distinct categories based on their biological functions and subcellular localization. Gene ontology analysis revealed that the 93 identified proteins could be functionally classified into nine groups including cytoskeleton (27%), signal transduction (12%), redox regulation (11%), proliferation and apoptosis (10%), metabolism (10%), and other functions (30%) (Fig. 1*C*). The majority of these proteins (55%) were located in the cytoplasm, and the remainder were situated either in the nuclear or cell membrane (Fig. 1*B*). For a macroscopic view, protein interactions and functional networks of up-regulated proteins (Fig. 1*G*) and down-regulated proteins

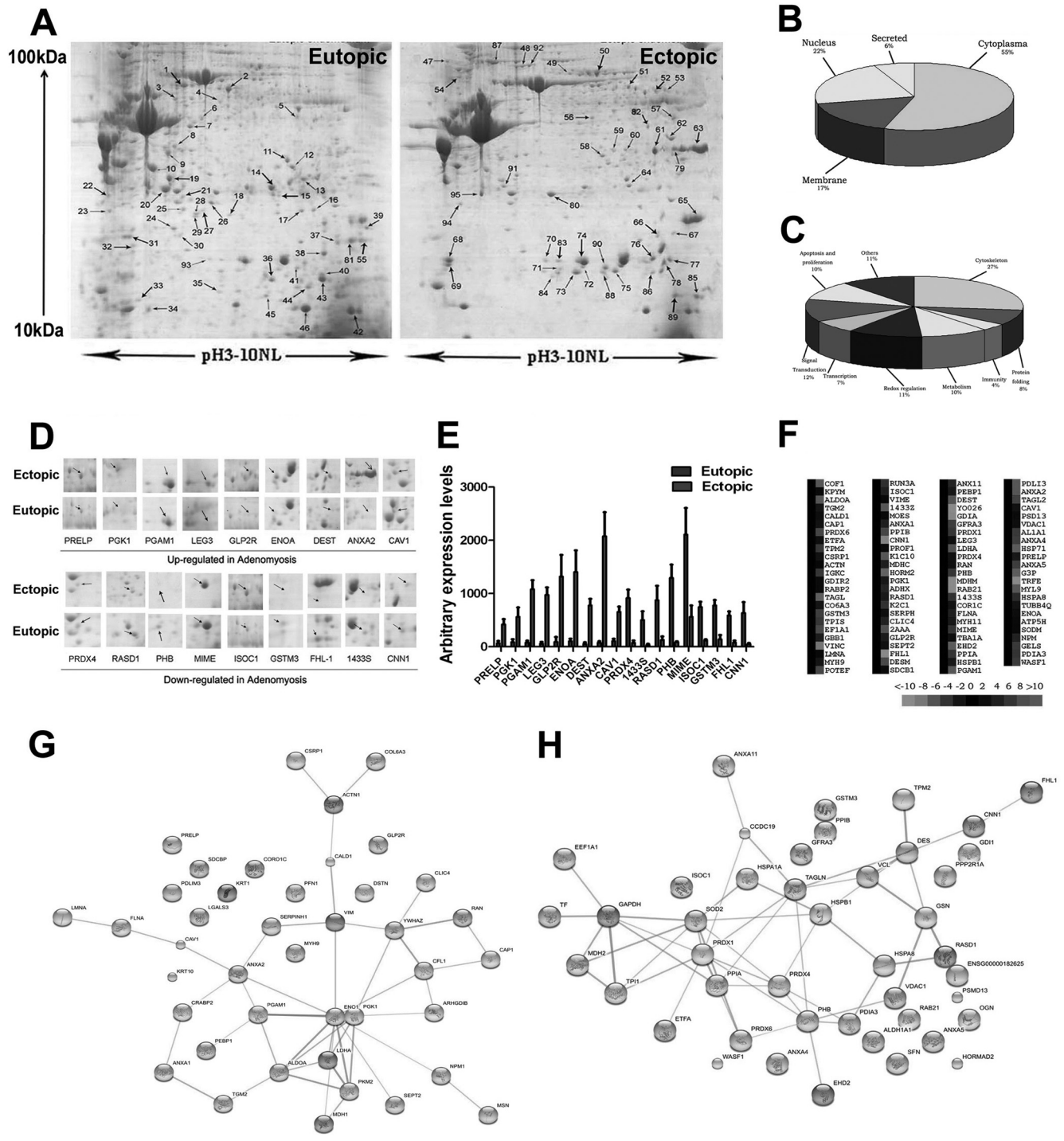

FIG. 1. **Proteomics analysis of differentially expressed proteins in matched ectopic and eutopic endometrium in human adenomyosis.** *A*, representative 2-DE maps of ectopic endometrium compared with matched eutopic endometrium in human adenomyosis. *B*, the identified proteins were categorized into several protein groups according to their subcellular locations. 55% of the total proteins were located in the cytoplasm, and the remainder were situated either in the nuclear or cell membrane. *C*, 93 identified proteins were functionally classified into nine groups. Many were involved in cytoskeleton (27%), signal transduction (12%), redox regulation (11%), proliferation and apoptosis (10%), metabolism (10%), and other functions (30%). *D*, expression profile of the 18 significantly altered proteins. The selected area was symmetrically boxed, and *arrows* indicate each protein spot or its theoretical location. *E*, the arbitrary expression values of the 18 significantly altered proteins were quantified using PDQuest 2-DE analysis software. *F*, protein cluster map generated by Cluster software. Expression of proteins in the normal group was constant at 0, whereas proteins up-regulated in the ectopic endometrium are in *red*, and the down-regulated proteins are in *green*. The intensity of the color *green* or *red* corresponds to the degree of alteration, respectively, according to the *color strip*

(Fig. 1*H*) were generated using the web-based tool String software, respectively. Interestingly, among the 93 proteins identified, 22 proteins, accounting for 23.7% of the total identified proteins, were found to be estrogen-responsive (Table III), as revealed by Kyoto Encyclopedia of Genes and Genomes pathway analysis. Of these, ANXA2 was the most remarkably up-regulated in the ectopic endometrium of adenomyosis compared with its matched eutopic counterpart (31.58-fold change, $p < 0.05$) (Fig. 1*E*).

Overexpression of ANXA2 in Ectopic Endometrium Is Correlated with EMT Markers and Dysmenorrhea Severity in Human Adenomyosis—As previous studies reported the critical role of ANXA2 in mediating cellular motility and proliferation in both normal (22) and malignant cells (23), our study further validated the expression level of ANXA2 in ectopic endometrial lesion lysates and lysates from matched eutopic endometrial tissues using immunoblotting. In good agreement with our 2-DE-derived data, the level of ANXA2 expression was significantly higher in ectopic endometrial lesions than the corresponding eutopic endometrial tissues ($n = 6$; Fig. 2*A*). Further immunohistochemistry assay in 65 pairs of matched ectopic and eutopic endometrium of adenomyosis revealed that the immunoreactivity of ANXA2 was consistently more intense and present in a higher portion of cells from the ectopic endometrial tissues than their eutopic counterparts regardless of either proliferative phase or secretory phase ($n = 65$, $p < 0.0001$; Fig. 2, *B* and *C*).

For external validation, publicly accessible microarray data from three data sets in NCBI Gene Expression Omnibus investigating differential gene expression in endometriosis, a gynecological disorder with similar pathology and pathogenesis as adenomyosis, were obtained (Table IV) (24–26). ANXA2 expression was significantly increased in ectopic endometrium compared with its eutopic counterpart in data set GSE5108 ($n = 22$, $p = 0.0463$; Fig. 2*D* and Table IV) and GSE6364 ($n = 37$, $p = 0.0447$; Fig. 2*D* and Table IV). In addition, an inverse relationship between ANXA2 and E-cadherin (encoded by CDH1) expression in publicly available data sets of endometriosis was noted (GSE5108 and GSE7305, $p = 0.0019$ and $p < 0.0001$, respectively, Table IV). Because E-cadherin is a vital player in mediating EMT (27), we further examined whether ANXA2 overexpression favors mesenchymal transcriptional programs in adenomyosis. Immunoblotting of ectopic endometrial lesion lysates and lysates from matched eutopic endometrial tissues of six individual adenomyosis patients for the expression level of E-cadherin and vimentin showed that the expression of E-cadherin was significantly down-regulated ($n = 6$; Fig. 2*A*), whereas vimentin expression was significantly elevated ($n = 6$; Fig. 2*A*) in the ectopic endometrial tissue lysates compared with their eutopic counterparts, suggesting the involvement of EMT process in the pathogenesis of adenomyosis. Further immunohistochemistry with antibodies against E-cadherin and vimentin in 65 pairs of paraffin-embedded specimens also indicated decreased expression of E-cadherin ($p < 0.0001$) and increased expression of vimentin ($p < 0.0001$) in ectopic endometrium compared with matched eutopic endometrium of adenomyosis ($n = 65$; Fig. 2, *B* and *C*).

Because dysmenorrhea was reported to be the second most prevalent symptom (30), we further analyzed the potential relationship between ANXA2 expression levels in the ectopic lesion and dysmenorrhea severity in adenomyosis patients. Our data demonstrated that ANXA2 expression was significantly higher in the ectopic lesions of adenomyosis patients who reported severe dysmenorrhea than those reporting no, mild, or moderate dysmenorrhea ($p < 0.0001$; Fig. 2*F*). Pearson correlation analysis identified a positive correlation between ANXA2 expression (adjusted by menstrual phase) of ectopic endometrium with dysmenorrhea scores in 40 patients with adenomyosis ($r^2 = 0.6969$; $p < 0.001$, Pearson χ^2 test; Fig. 1*E*). In addition, a positive correlation between ANXA2 expression in ectopic endometrium and serum CA12-5 level, a marker indicative of adenomyosis severity, in adenomyosis patients was also noted ($r^2 = 0.1771$, $p = 0.0206$, Pearson χ^2 test; Fig. 1*G*).

E2 Induces Up-regulation of ANXA2 and EMT in Endometrial Cells—It is well established that high serum estrogen concentration contributes to adenomyosis development (17). Thus, we examined whether E2 could result in up-regulation of ANXA2 in ISK cells (a well differentiated endometrial cell line that expresses estrogen and progesterone receptors and is one of the best available *in vitro* models for the investigation of adenomyosis) (17) and induce EMT. As shown in Fig. 3 (*A* and *C*), E2 treatment led to a significant up-regulation of ANXA2 as demonstrated by RT-PCR, immunoblotting, and immunofluorescence microscopy. More interestingly, ISK cells treated with E2 showed an elongated, epithelial morphology compared with its original shape (Fig. 3*B*), which suggested that these cells underwent rearrangement of the cytoskeleton, implicating the occurrence of EMT (28). Furthermore, this morphological change was accompanied by marked reduction of E-cadherin expression and increased expression of vimentin and slug (Fig. 3, *A* and *C*). These effects could be effectively reversed by the treatment of tamoxifen (TAM), an antagonist of estrogen receptor. Taken together, these results implicated that E2 is a potent EMT inducer through up-regulation of ANXA2 in endometrial cells of adenomyosis.

at the *bottom* of the figure. *G*, the protein-protein interaction network of identified up-regulated proteins in ectopic endometrium in adenomyosis compared with matched eutopic endometrium analyzed by String software. *H*, the protein-protein interaction network of identified down-regulated proteins in ectopic endometrium in adenomyosis compared with matched eutopic endometrium analyzed by String software. All of the data are shown as the means ± S.D.

TABLE II
Identified proteins by ESI-Q-TOF

Spot No.	Accession No.[a]	Protein name[b]	Gene name	Exp molecular mass[c]	Theoretical molecular mass	Exp pI[c]	Theoretical pI	No. of Peptides	Coverage (%)	Score[d]
1	P18206	Vinculin	VCL	124,292	123,799	5.5	5.5	3	4	61
2	Q8N7B1	HORMA domain-containing protein 2	HORMAD2	35,718	35,284	6.86	6.86	2	2	56
3	Q92558	Wiskott-Aldrich syndrome protein family member 1	WASF1	61,899	61,652	6.01	6.01	2	3	38
4	P01834	Ig κ chain C region	IGKC	11,773	11,609	5.58	5.58	18	32	74
5	P50995	Annexin A11	ANAX11	54,697	54,390	7.53	7.53	2	3	42
6	Q9UNM6	26 S proteasome non-ATPase regulatory subunit 13	PSMD13	43,176	42,945	5.53	5.53	2	3	38
7	Q59EK9	RUN domain-containing protein 3A	RUNDC3A	50,172	49,747	5.19	5.19	2	3	267
8	P02545	Lamin-A/C	LMNA	74,380	74,139	6.57	6.57	8	19	247
9	P62873	Guanine nucleotide-binding protein G(I)/G(S)/G(T) subunit β-1	GNB1	38,151	37,377	5.6	5.6	6	13	206
10	A5A3E0	POTE ankyrin domain family member F	POTEF	123,020	121,445	5.83	5.82	3	4	175
11	Q9Y272	Dexamethasone-induced Ras-related protein 1	RASD1	32,021	31,642	9.15	9.15	2	3	108
12	Q96CN7	Isochorismatase domain-containing protein 1	ISOC1	32,501	32,237	6.96	6.96	15	28	58
13	O60609	GDNF family receptor α-3	GFRA3	46,134	44,511	8.06	8.06	4	7	120
14	P30041	Peroxiredoxin-6	PRDX6	25,133	25,035	6.01	6.0	21	77	765
15	P30153	Serine/threonine-protein phosphatase 2A 65-kDa regulatory subunit A α isoform	PPP2R1A	66,065	65,309	5.0	5.0	12	26	755
16	P68104	Elongation factor 1-α 1	EEF1A1	50,451	50,141	9.1	9.1	3	5	703
17	P04179	Superoxide dismutase (Mn), mitochondrial	SOD2	24,878	24,722	8.35	8.35	27	47	684
18	P08670	Vimentin	VIM	53,676	53,652	5.06	5.05	12	17	665
19	Q9Y696	Chloride intracellular channel protein 4	CLIC4	28,982	28,772	5.45	5.45	4	7	543
20	P35749	Myosin-11	MYH11	24,976	24,976	6.54	6.54	3	4	508
21	Q13162	Peroxiredoxin-4	PRDX4	30,749	30,540	5.86	5.86	15	39	506
22	P07951	Tropomyosin β chain	TPM2	32,945	32,851	4.66	4.66	8	13	414
23	P17661	Desmin	DES	53,560	53,536	5.21	5.21	12	23	109
24	P00352	Retinal dehydrogenase 1	ALDH1A1	55,454	54,862	6.3	6.3	22	31	170
25	P30101	Protein disulfide-isomerase A3	PDIA3	57,146	56,782	5.98	5.98	3	5	39
26	P08107	Heat shock 70-kDa protein 1	HSPA1A	70,294	70,052	5.48	5.47	21	24	304
27	P09525	Annexin A4	ANXA4	36,088	35,883	5.84	5.83	16	30	262
28	P60174	Triosephosphate isomerase	TPI1	26,938	30,791	6.45	5.65	7	48	36
29	P06396	Gelsolin	GSN	86,043	85,698	5.9	5.9	4	17	55
30	Q71U36	Tubulin α-1A chain	TUBA1A	50,788	50,136	4.94	4.94	9	12	256
31	P21266	Glutathione *S*-transferase Mu 3	GSTM3	26,998	26,560	5.37	5.37	3	7	61
32	P06748	Nucleophosmin	NPM1	32,726	32,575	4.64	4.64	6	9	45
33	P08758	Annexin A5	ANXA5	35,971	35,937	4.94	4.93	3	5	57
34	Q9UL25	Ras-related protein Rab-21	RAB21	24,731	24,348	8.11	8.11	5	5	44
35	P04792	Heat shock protein β-1	HSPB1	22,826	22,783	5.98	5.98	21	80	304
36	Q01995	Transgelin	TAGLN	22,653	22,551	8.87	8.87	15	46	117
37	P51911	Calponin-1	CNN1	33,321	33,170	9.14	9.14	8	22	165
38	P23528	Cofilin-1	CFL1	18,719	18,502	8.22	8.22	9	16	77
39	P23284	Peptidyl-prolyl *cis-trans*-isomerase B	PPIB	23,785	23,743	9.42	9.42	6	11	56
40	P62937	Peptidyl-prolyl *cis-trans*-isomerase A	PPIA	18,229	18,012	7.68	7.68	36	50	130
41	Q9NZN4	EH domain-containing protein 2	EHD2	61,294	61,161	6.03	6.02	6	9	129
42	P04406	Glyceraldehyde-3-phosphate dehydrogenase	GAPDH	36,201	36,053	8.57	8.57	21	35	129

TABLE II—*continued*

Spot No.	Accession No.[a]	Protein name[b]	Gene name	Exp molecular mass[c]	Theoretical molecular mass	Exp pI[c]	Theoretical pI	No. of Peptides	Coverage (%)	Score[d]
43	P40926	Malate dehydrogenase, mitochondrial	MDH2	35,937	35,503	8.92	8.92	3	5	209
44	P37802	Transgelin-2	TAGLN2	22,548	22,391	8.41	8.41	9	45	76
45	P35232	Prohibitin	PHB	29,843	29,804	5.57	5.57	8	10	104
46	P20774	Mimecan	OGN	34,243	33,922	5.46	5.46	3	9	96
47	P12111	Collagen α-3(VI) chain	COL6A3	345,163	343,669	6.26	6.26	11	12	92
48	P21333	Filamin-A	FLNA	283,301	280,739	5.7	5.7	6	7	70
49	Q05682	Caldesmon	CALD1	93,251	93,231	5.63	5.62	2	2	81
50	Q15019	Septin-2	SEPT2	41,689	41,487	6.15	6.15	15	34	77
51	Q9ULV4	Coronin-1C	CORO1C	53,899	53,249	6.65	6.65	4	16	64
52	P51888	Prolargin	PRELP	44,181	43,810	9.47	9.47	8	9	83
53	O95838	Glucagon-like peptide 2 receptor	GLP2R	63,873	63,001	9.1	9.1	2	2	70
54	P31150	Rab GDP dissociation inhibitor α	GDI1	51,177	50,583	5.0	5.0	18	29	184
55	Q13642	Four and a half LIM domains protein 1	FHL1	38,006	36,263	9.25	9.25	5	8	56
56	P61163	α-Centractin	ACTR1A	42,701	42,614	6.19	6.19	21	38	67
57	P00558	Phosphoglycerate kinase 1	PGK1	44,985	44,615	8.3	8.3	3	47	66
58	P04083	Annexin A1	ANXA1	38,918	38,714	6.57	6.57	11	32	125
59	P14618	Pyruvate kinase isozymes M1/M2	PKM2	58,470	57,937	7.96	7.96	8	9	256
60	P40925	Malate dehydrogenase, cytoplasmic	MDH1	36,631	36,426	6.91	6.91	15	16	61
61	Q53GG5	PDZ and LIM domain protein 3	PDLIM3	39,835	39,232	6.42	6.42	6	9	549
62	P04075	Fructose-bisphosphate aldolase A	ALDOA	39,851	39,420	8.3	8.3	15	39	171
63	P07355	Annexin A2	ANXA2	38,808	38,604	7.57	7.57	18	78	254
64	P11766	Alcohol dehydrogenase class-3	ADH5	40,554	39,724	7.45	7.45	8	12	56
65	P21291	Cysteine- and glycine-rich protein 1	CSRP1	21,409	20,567	8.9	8.9	32	48	326
66	P13804	Electron transfer flavoprotein subunit α, mitochondrial	ETFA	35,400	35,080	8.62	8.62	6	8	175
67	P30086	Phosphatidylethanolamine-binding protein 1	PEBP1	21,158	21,057	7.01	7.01	17	55	56
68	P63104	14-3-3 protein ζ/δ	YWHAZ	27,899	27,745	4.73	4.73	6	36	45
69	P13645	Keratin, type I cytoskeletal 10	KRT10	59,046	58,827	5.09	5.13	2	23	342
70	O75947	ATP synthase subunit d, mitochondrial	ATP5H	18,537	18,491	5.21	5.21	3	13	202
71	P29373	Cellular retinoic acid-binding protein 2	CRABP2	15,854	15,693	5.42	5.38	21	55	42
72	P21980	Protein-glutamine gamma-glutamyltransferase 2	TGM2	34,620	77,329	5.13	5.11	9	29	269
73	P24844	Myosin regulatory light polypeptide 9	MYL9	19,871	19,827	4.8	4.78	8	67	49
74	P18669	Phosphoglycerate mutase 1	PGAM1	28,900	28,804	6.67	6.67	6	77	157
75	P04264	Keratin, type II cytoskeletal 1	KRT1	66,170	66,039	8.15	8.15	4	6	75
76	P50454	Serpin H1	SERPINH1	46,525	46,441	8.75	8.75	14	46	469
77	P23528	Cofilin-1	CFL1	18,719	18,502	8.22	8.22	9	42	49
78	P60981	Destrin	DSTN	18,950	18,506	8.06	8.06	18	45	165
79	P00338	L-Lactate dehydrogenase A chain	LDHA	36,950	36,689	8.44	8.44	4	17	337
80	P26038	Moesin	MSN	67,892	67,820	6.08	6.08	8	15	57
81	P21796	Voltage-dependent anion-selective channel protein 1	VDAC1	30,868	30,773	8.62	8.62	4	7	50
82	Q01518	Adenylyl cyclase-associated protein 1	CAP1	52,222	51,901	8.27	8.24	6	30	265
83	P52566	Rho GDP-dissociation inhibitor 2	ARHGDIB	23,031	22,988	5.1	5.08	8	43	184
84	Q06830	Peroxiredoxin-1	PRDX1	22,049	22,110	5.66	8.27	19	44	343
85	P07737	Profilin-1	PFN1	15,216	15,054	8.44	8.44	9	57	135

TABLE II—*continued*

Spot No.	Accession No.[a]	Protein name[b]	Gene name	Exp molecular mass[c]	Theoretical molecular mass	Exp pI[c]	Theoretical pI	No. of Peptides	Coverage (%)	Score[d]
86	P62826	GTP-binding nuclear protein Ran	RAN	24,579	24,423	7.01	7.01	3	6	592
87	P35579	Myosin-9	MYH9	227,646	226,532	5.5	5.5	9	73	58
88	O00560	Syntenin-1	SDCBP	32,595	32,444	7.05	7.06	7	18	129
89	P17931	Galectin-3	LGALS3	26,193	26,152	8.57	8.58	4	15	67
90	P06733	α-Enolase	ENO1	47,481	47,169	7.01	7.01	38	43	114
91	Q03135	Caveolin-1	CAV1	20,472	20,472	5.64	5.64	27	32	293
92	P12814	α-Actinin-1	ACTN1	103,058	103,058	5.25	5.25	5	7	88
93	P31947	14-3-3 protein σ	SNF	27,774	27,774	4.73	4.68	18	26	129

[a] Accession numbers were obtained from the ExPASy database.
[b] Multiple isoforms of these proteins were identified in the same individual.
[c] Theoretical molecular mass (Da) and pI were from the ExPASy database.
[d] Probability-based MOWSE scores.

TABLE III
Estrogen-responsive proteins altered in adenomyosis

Spot No.	Protein name	Accession No.	Average ratio (EC/EU)[a]	Subcellular location[b]	Biological function[c]
9	Guanine nucleotide-binding protein G(I)/G(S)/G(T)subunit beta-1	P62873	0.22	Cytoplasm	Cell signaling/redox homeostasis
14	Peroxiredoxin-6	P30041	0.1	Cell membrane	Redox homeostasis
19	Chloride intracellular channel protein 4	Q9Y696	0.13	Mitochondrion	Angiogenesis/redox homeostasis
21	Peroxiredoxin-4	Q13162	0.35	Nucleus	Redox homeostasis
26	Heat shock 70-kDa protein 1	P08107	0.082	Cytoplasm	Cell proliferation
27	Annexin A4	P09525	0.12	Melanosome	Apoptosis cell signaling
29	Gelsolin	P06396	0.12	Cytoplasm	Cell proliferation/cell motility
32	Nucleophosmin	P06748	7.13	Cell membrane	Cell proliferation/cell motility/cell adhesion
37	Calponin-1	P51911	0.064	Cytoplasm	Angiogenesis/cell motility
45	Prohibitin	P35232	0.13	Cytoplasm	Cell proliferation/cell adhesion
48	Filamin-A	P21333	7.31	Cell membrane	Cell motility
55	Four and a half LIM domain proteins 1	Q13642	0.063	Cytoplasm	Cell proliferation
58	Annexin A1	P04083	7.35	Nucleus; cytoplasm	Apoptosis
63	Annexin A2	P07355	31.58	Cytoplasm	Cell proliferation
80	Moesin	P26038	2.53	Cell membrane	Cell adhesion/cell motility
81	Voltage-dependent anion-selective channel protein 1	P21796	0.39	Mitochondrion outer membrane; cell membrane	Apoptosis
84	Peroxiredoxin-1	Q06830	7.13	Cytoplasm; melanosome	Redox homeostasis/cell proliferation
86	GTP-binding nuclear protein Ran	P62826	3.58	Nucleus; cytoplasm; melanosome.	Cell proliferation/cell signaling
89	Galectin-3	P17931	3.89	Nucleus	Angiogenesis
91	Caveolin-1	Q03135	2.22	Membrane	Angiogenesis/cell proliferation/ cell signaling
92	α-Actinin-1	P12814	2.34	Cytoplasm	Cell proliferation
93	14-3-3 protein σ	P31947	0.19	Cytoplasm	Cell proliferation/cell signaling

[a] Ectopic endometrium (EC) versus eutopic endometrium (EU).
[b] Information of subcellular location from the ExPASy database.
[c] Information of biological function from ExPASy database and Kyoto Encyclopedia of Genes and Genomes pathway database.

Enforced Expression of ANXA2 in Human Endometrial Cells Induces EMT and Increases Cell Proliferation in Vitro in a β-Catenin/Tcf Signaling-associated Manner—We next investigated whether enforced expression of ANXA2 could induce EMT in endometrial cells. A stable ISK cell line overexpressing ANXA2 (designated ISK^{ANXA2} cells) and a stable ISK cell line overexpressing NC (designated ISK^{NC} cells) were established. We found that although the control ISK cells retained an epithelial morphology with tight cell to cell adhesion, ISK^{ANXA2} cells displayed an elongated morphology typically associated

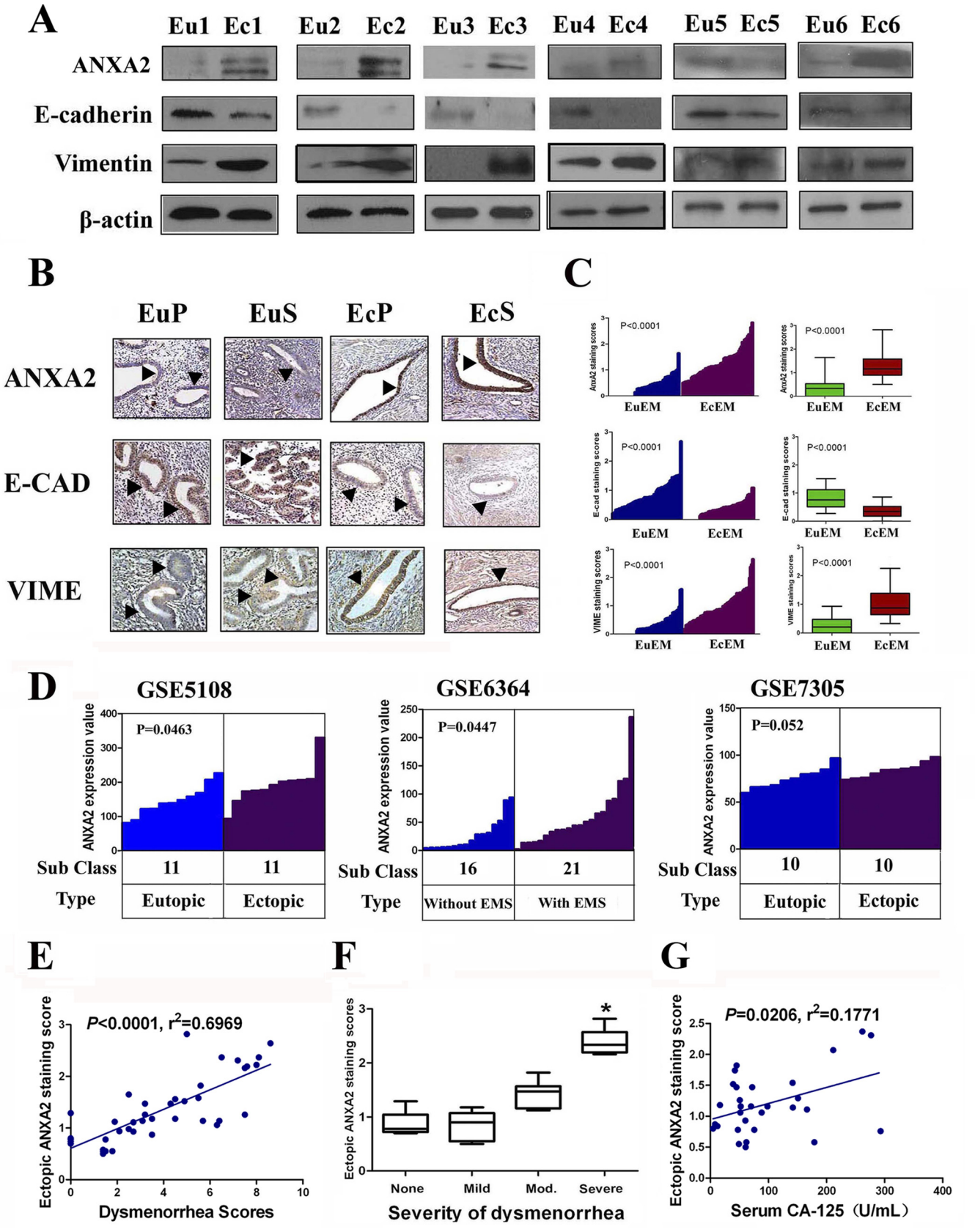

10.1074/mcp.M112.017988–11

TABLE IV
Publicly available microarray data sets of endometriosis patients analyzed for the relevant role of ANXA2 (annexin A2) and CDH1 (E-cadherin)

Data set	Gene	Control (*n*)	Endometriosis (*n*)	*p* value (*t* test)	GSE No.
Eyster Km (PMID:17462640)[a]	ANXA2	145.86 (11)	192.14 (11)	0.0463	GSE5108
	CDH1	16.90 (11)	6.62 (11)	0.0019	
Burney RO (PMID:17510236)[b]	ANXA2	27.71 (16)	58.52 (21)	0.0447	GSE6364
Hever A (PMID:17640886)[c]	ANXA2	75.10 (10)	83.94 (10)	0.052	GSE7305
	CDH1	961.40 (10)	152.03 (10)	<0.0001	

[a] Whole human genome DNA microarray analysis of gene expression in ectopic *versus* eutopic endometrium loci.
[b] Gene profiling of endometrium reveals progesterone resistance and candidate genetic loci in women with endometriosis.
[c] Human endometriosis *versus* normal endometrium study-transcriptional profiling.

TABLE V
Primer sequences for selected genes

Gene	Sequences	Annealing temperature (°C)
ANXA2	Sense 5′-GTGGATGAGGTCACCATTGTC-3′ Antisense 5′-GTCGGTTCCTTTCCTCTTCAC-3′	58
c-Myc	Sense 5′-TGAAAGGCTCTCCTTGCAGC-3′ Antisense 5′-GCTGGTAGAAGTTCTCCTCC-3′	58
Cyclin D1	Sense 5′-ATGTGTGCAGAAGGAGGTCC-3′ Antisense 5′-CTTAGAGGCCACGAACATGC-3′	61
c-Jun	Sense 5′-AACCTCAGCAACTTCAACCC-3′ Antisense 5′-CTTCCTTTTTCGGCACTTGG-3′	56
MMP-7	Sense 5′-AGATCCCCCTGCATTTCAGG-3′ Antisense 5′-TCGAAGTGAGCATCTCCTCC-3′	61
GAPDH	Sense 5′-ACCACAGTCCATGCCATCAC-3′ Antisense 5′-TCCACCACCCTGTTGCTGTA-3′	60

with mesenchymal phenotype (Fig. 4*B*). Furthermore, immunoblotting and immunofluorescence analyses indicated increased expression of vimentin and slug and diminished expression of E-cadherin in ISK^{ANXA2} cells compared with the control ISK cells (Fig. 4, *A* and *C*). We further explored the effects of enforced expression ANXA2 on the proliferation capacity of endometrial cell lines. ISK^{ANXA2} cells formed significantly more colonies than control cells did, which indicated enhanced proliferation capacity (Fig. 4*D*).

In canonical Wnt pathways, β-catenin nuclear localization was prevented by E-cadherin binding when Wnt signaling pathway is inactivated. However, the loss of E-cadherin, together with inhibition of GSK-3β-mediated β-catenin degradation, could lead to accumulation of β-catenin in the nucleus that further transactivates β-catenin/Tcf target genes. Because enforced ANXA2 expression in ISK cells resulted in a robust decrease in E-cadherin expression, we next investigated whether β-catenin/Tcf/Lef signaling pathway was activated in ISK^{ANXA2} cells. TOP/FOP-flash assay indicated that the relative transcriptional activity of the β-catenin/Lef complex was induced in ISK^{ANXA2} cells compared with ISK^{NC} cells ($p < 0.05$; Fig. 4*E*). Moreover, we further examined the mRNA levels of four well characterized β-catenin target genes including c-Myc, cyclin D1, c-Jun, and MMP-7 (Table V) (28) and found that c-Myc, c-Jun, and MMP-7 were significantly up-regulated in ISK^{ANXA2} cells and LiCl-treated ISK cells compared with control (Fig. 4*F*). Hence, our data proved that enforced expression of ANXA2 could induce EMT and increase cell proliferation *in vitro* via activating β-catenin/Tcf signaling pathway in ISK cells.

ANXA2 Depletion Reverses the Phenotype of Invasion and Metastasis in Endometrial Cells in Vitro—To test whether

FIG. 2. **Overexpression of ANXA2 in ectopic endometrium is correlated with EMT markers and dysmenorrhea severity in human adenomyosis.** *A*, matched eutopic (*Eu1–Eu6*) and ectopic (*Ec1–Ec6*) endometrial tissues separately obtained from six adenomyosis patients were analyzed for ANXA2, E-cadherin, and vimentin by immunoblotting. β-Actin was used as a loading control. *B*, matched eutopic and ectopic endometrial tissues either in proliferative phase (*EuP* and *EcP*) or secretory phase (*EuS* and *EcS*) were analyzed for ANXA2, E-cadherin, and vimentin by immunohistochemistry. *C*, ANXA2, E-cadherin, and vimentin expression in matched eutopic and ectopic endometrium of adenomyosis were plotted using the IHC staining scores ($n = 65$). *D*, ANXA2 expression levels in ectopic endometrium compared with eutopic endometrium or in eutopic endometrium of females with endometriosis compared with eutopic endometrium of females without endometriosis in three NCBI Gene Expression Omnibus covered microarray data sets. *E*, correlation between ectopic ANXA2 staining scores and dysmenorrhea scores in 40 adenomyosis patients with linear regression lines and Pearson correlation significance. *F*, box plot of immunoreactivity of ectopic ANXA2 expression and severity of dysmenorrhea in adenomyosis. *Mod.* stands for moderate. *G*, correlation between ectopic ANXA2 staining scores and serum CA12-5 levels in 30 adenomyosis patients with linear regression lines and Pearson correlation significance. *, $p < 0.05$; **, $p < 0.01$; ***, $p < 0.001$.

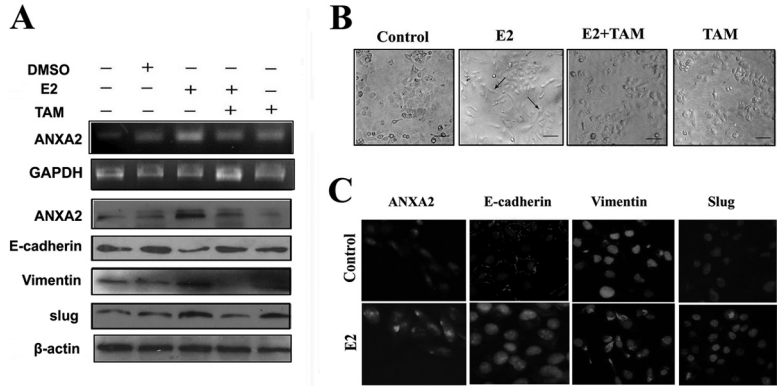

FIG. 3. **ANXA2 mediates E2-induced EMT in ISK cells.** *A*, ISK cells treated with DMSO, E2, TAM, or E2 + TAM were analyzed for mRNA level of ANXA2 by RT-PCR and protein expression levels of ANXA2, E-cadherin, vimentin, and slug by immunoblotting. GAPDH and β-actin were used as loading controls in RT-PCR and immunoblotting, respectively. *B*, representative phase contrast images of cell morphology in DMSO-, E2-, E2 + TAM-, and TAM-treated ISK cells. *C*, double immunofluorescence localization of ANXA2, E-cadherin, vimentin, and slug in DMSO- or E2-treated ISK cells. The cells were stained for ANXA2, E-cadherin, vimentin, and slug, respectively, and counterstained with DAPI to visualize the nuclei.

ANXA2 is indispensable for the invasiveness of endometrial cells, we introduced siRNA to knock down ANXA2 expression in ISK cells. Immunoblotting and immunofluorescence analyses indicated a decrease in the expression of vimentin but a robust increase in E-cadherin expression (Fig. 5, *A* and *B*) in $ISK^{siANXA2}$ cells compared with control. Although siRNA-mediated repression of ANXA2 did not affect morphology of ISK cells, siRNA-transfected ISK cells showed reduced proliferation compared with control cells, cells transfected with empty vector alone, or cells transfected with negative control, as measured by MTT cell proliferation assays ($p < 0.05$; Fig. 5*C*). Additionally, both monolayer wound healing assay ($p < 0.05$; Fig. 5*D*) and Transwell chamber migration assay ($p < 0.0001$; Fig. 5*G*) indicated significantly decreased migration capacity of $ISK^{siANXA2}$ cells compared with $ISK^{control}$ cells. Using a Transwell chamber invasion assay, we observed a significant decrease in the invasive capacity of $ISK^{siANXA2}$ cells compared with $ISK^{control}$ cells ($p < 0.05$; Fig. 5*H*).

To determine cell survival independent of cell adhesion, we examined the effect of inhibition of ANXA2 on anoikis, an established model of apoptosis resulting from loss of cell matrix interaction (29). Interestingly, knockdown of ANXA2 in ISK cells resulted in significant increase in cell death (Fig. 5*E*) and decrease in percentage of viable cells because of anoikis (Fig. 5*F*). As shown in Fig. 5*E*, $ISK^{siANXA2}$ demonstrated significantly increased apoptosis compared with $ISK^{control}$ because of anoikis challenge (15.17% *versus* 2.73%, respectively). Therefore, the above data indicated that ANXA2 plays a critical role in the regulation of growth, migration, invasion, and anoikis resistance in adenomyotic endometrial cells.

Overexpression of ANXA2 in Adenomyotic Endometrial Cells Contributes to Enhanced Angiogenesis via HIF-1α/VEGF-A Signaling Pathway—After migrating to an ectopic location, endometrial cells function in regulating local angiogenesis (10). Previous studies have identified HIF-1α/VEGF-A signaling as one of the major pathways involved in angiogenesis regulation (9), and hence we examined whether HIF-1α/VEGF-A signaling pathway is activated in the ectopic endometrium during adenomyosis development. Immunohistochemistry analysis of 65 pairs of matched ectopic and eutopic endometrial specimens in adenomyosis revealed that HIF-1α ($n = 65$, $p < 0.001$; Fig. 6*A*) and its target VEGF-A ($n = 65$, $p = 0.005$; Fig. 6*A*) were significantly overexpressed in ectopic endometrium of adenomyosis compared with its corresponding eutopic endometrium. Although the expression of HIF-1α was predominantly restricted to the nuclei of both epithelial and stromal endometrial cells of ectopic foci (Fig. 6, *A* and *B*), intense VEGF-A immunostaining was noted mainly in the ectopic endometrial cells when compared with eutopic endometrial cells (Fig. 6, *A* and *B*), which indicated activation of HIF-1α/VEGF-A pathway in the ectopic endometrium of adenomyosis. To further investigate whether the activated HIF-1α/VEGF-A pathway was associated with enhanced local neovascularization, we evaluated microvessel density in different sections stained with an antibody reactive to CD31 and found that either in the proliferative or secretory phase, the ectopic endometrium consistently demonstrated higher microvessel density than its matched eutopic counterpart ($n = 65$, $p < 0.0001$; Fig. 6*A*). *In vitro*, we assessed the expression levels of HIF-1α and VEGF-A by immunoblotting and immunofluorescence assay in $ISK^{control}$ cells and ISK^{ANXA2} cells and observed that enforced expression of ANXA2 increased HIF-1α and VEGF-A expression significantly (Fig. 6, *C* and *D*). These data implicated that overexpression of ANXA2 could provoke remarkable up-regulation of HIF-1α and VEGF-A.

To further explore the role of ANXA2 in regulating the proangiogenic capacity of endometrial cells, the effects of secreted factors from $ISK^{control}$ and ISK^{ANXA2} cell cultures on vascular endothelial cells (HUVEC) *in vitro* were investigated. We first

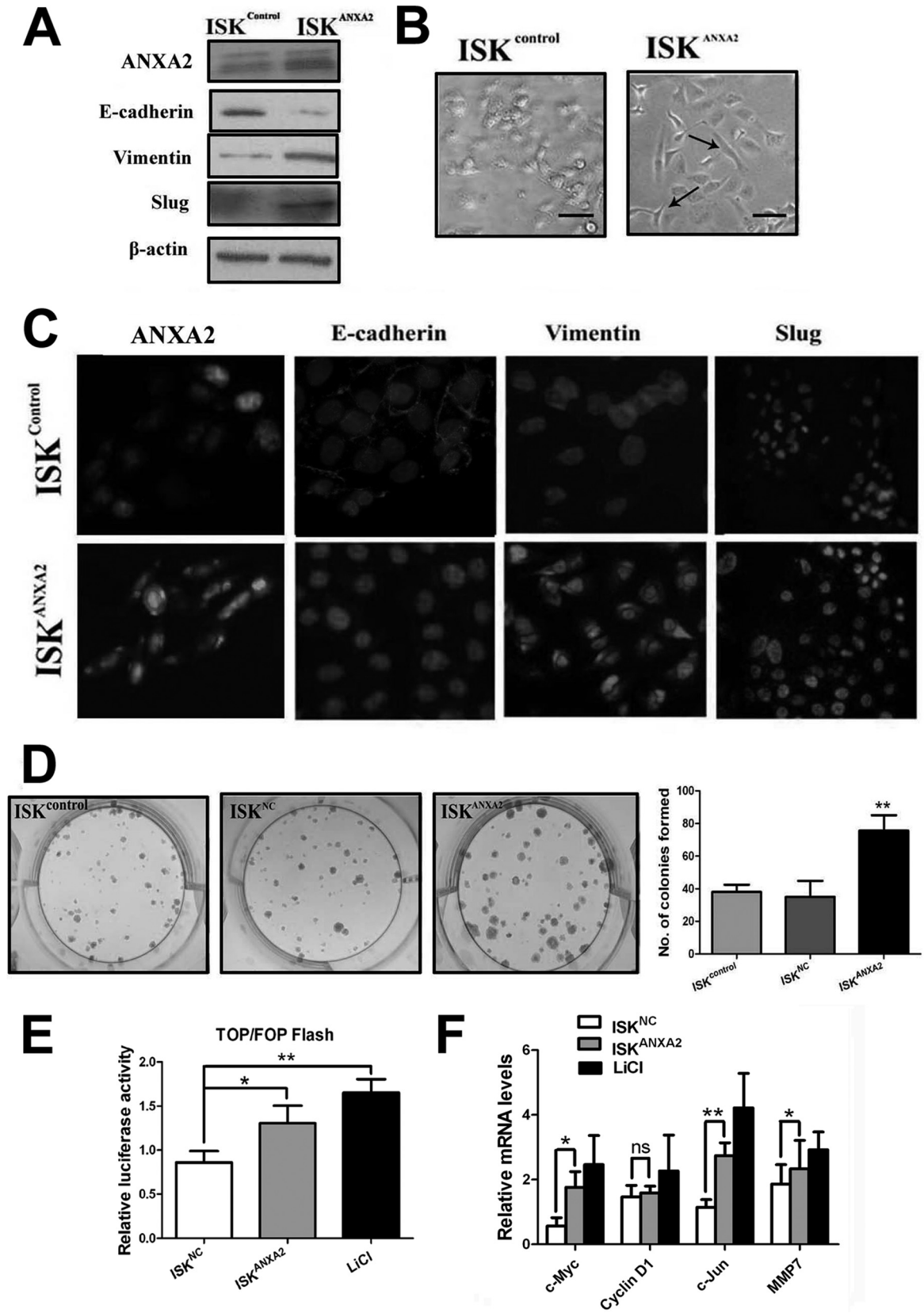
A
ISK Control
ISK ANXA2
ANXA2
E-cadherin
Vimentin
Slug
β-actin
B
ISK control
ISK ANXA2
C
ANXA2
E-cadherin
Vimentin
Slug
ISK Control
ISK ANXA2
D
ISK control
ISK NC
ISK ANXA2
No. of colonies formed
100
80
60
40
20
0
**
ISK control
ISK NC
ISK ANXA2
E
TOP/FOP Flash
Relative luciferase activity
2.0
1.5
1.0
0.5
0.0
**
*
ISK NC
ISK ANXA2
LiCl
F
ISK NC
ISK ANXA2
LiCl
Relative mRNA levels
6
4
2
0
*
ns
**
*
c-Myc
Cyclin D1
c-Jun
MMP7

compared the level of VEGF in $ISK^{control}$ cell- and ISK^{ANXA2} cell-conditioned media and whole cell lysates using ELISA and immunoblotting analysis and found a significantly increased concentration of VEGF in both ISK^{ANXA2} cell conditioned media and whole cell lysates compared with $ISK^{control}$ cells ($p < 0.05$; Fig. 7, *A* and *B*). Incubation of HUVEC cells with ISK^{ANXA2} cell-conditioned medium for 48 h resulted in a significant increase of HUVEC cells compared with $ISK^{control}$ and ISK^{NC} cell conditioned media ($p < 0.05$; Fig. 7*C*), as measured by MTT assay. In addition, ISK^{ANXA2} cell culture medium enhanced the chemotactic rate of HUVEC cells ($p < 0.05$; Fig. 7*D*), as well as the morphological differentiation of HUVEC cells into tube-like vascular structures ($p < 0.05$; Fig. 7*E*). To determine whether ANXA2 is involved in angiogenesis of ectopic lesion in adenomyosis *in vivo*, we performed alginate-encapsulated cell assay. As shown in Fig. 7*F*, newborn blood vessels on alginate beads from nude mice treated with Lipo + ANXA2 shRNA were significantly fewer than those in other control groups ($p < 0.05$). Taken together, these data demonstrated an important role of ANXA2 in modulating proangiogenesis via activation of HIF-1α/VEGF-A pathway in adenomyotic endometrial cells.

ANXA2 Knockdown Compromises Growth, Metastasis, and Proangiogenesis of Adenomyotic Endometrial Cells and Alleviates Generalized Hyperalgesia in Vivo—To validate whether ANXA2 is critical for endometrial cell growth and metastasis *in vivo*, we established an experimental adenomyosis model in nude mice that mimics ectopic implantation of the endometrium. In mice treated with NS, Lipo, or Lipo + NC shRNA, measurable endometrial fragments after a 25-day incubation were observed, with an average volume of 28.36, 18.17, and 19.74 mm^3, respectively (Fig. 8, *A* and *F*). In addition, adenomyotic nodules in these groups were all red with small blood vessels visible. By contrast, endometrial fragments from mice treated with Lipo + ANXA2 shRNA could hardly be detectable after 25 days of growth (Fig. 8*A*). Four mice (57.1%) in this group even showed complete regression of adenomyotic lesions (Fig. 8, *B* and *E*). The average volume of adenomyotic nodules in this group was only 3.16 mm^3 at sacrifice (Fig. 8*F*). In addition, the average weight of endometrial nodules in the Lipo + ANXA2 shRNA-treated group was significantly lower than those in either NS, Lipo, or Lipo + NC shRNA-treated group ($p = 0.0004$; Fig. 8*G*). At the time of sacrifice, all control mice treated with NS, Lipo, or Lipo + NC shRNA showed persistence of active lesions with angiogenic and glandular organization (the scores were 2.10 ± 0.74, 2.30 ± 0.57, and 2.10 ± 0.55, respectively; Fig. 8*C*). By contrast, among the seven nude mice treated with Lipo + ANXA2 shRNA, four mice (57.1%) showed complete regression of adenomyotic lesions, with the remaining three mice displaying fibrotic and avascular lesions (score 1.10 ± 0.54; Fig. 8*C*). The pathology scores of the mice treated with Lipo + ANXA2 shRNA and the mice in the three control groups demonstrated significant differences ($p = 0.0271$; Fig. 8*D*). Also, the colors of the adenomyotic nodules in the three mice with adenomyotic lesions at the time of sacrifice in the treatment group were all pale with no blood vessels visible.

In addition, as Liu and Guo (30) reported that dysmenorrhea in adenomyosis patients stems from generalized hyperalgesia, we next assessed whether ANXA2 knockdown could attenuate the generalized hyperalgesia in this adenomyosis nude mice model. Mice that received Lipo + shANXA2 treatment for 20 days had a significant improvement in hot plate latency ($p < 0.0001$; Fig. 8*H*) and benefited from remarkable analgesic effects as compared with the control group mice ($p < 0.0001$; Fig. 8*I*). Hot plate responses of each nude mouse at 54 °C were recorded prior to the xenotransplantation of endometrial lesions (Test 1), prior to the initiation of treatment (Test 2), 15 days after the surgery (Test 3), and prior to the sacrifice of nude mice (Test 4). As expected, there were no differences in test 1 latency among the four groups ($p > 0.05$; Fig. 8*H*). However, 5 days after the surgery but prior to the initiation of respective treatments, the test 2 latency in all groups was significantly decreased as compared with that of Test 1 (Fig. 8*H*). This suggested that experimentally induced adenomyosis significantly lowered the tolerance to noxious thermal stimulus as compared with the base line, even though the location that received the stimulus was distant from the location where adenomyotic tissues were transplanted. However, we further found that mice that received Lipo + shANXA2 treatment for 20 days had a significant improvement in latency as compared with the control group mice prior to sacrifice ($p < 0.0001$; Fig. 8*H*). In addition, we performed the formalin test to assess the way adenomyosis nude mice model responds to continuous pain generated by injured tissue. The formalin test has a distinctive biphasic peripheral nociceptive response termed as the early and late phases. The early phase or tonic pain response corresponds to the

FIG. 4. **Enforced expression of ANXA2 induces EMT and enhances cell proliferation via β-catenin-Tcf signaling pathway.** *A*, immunoblotting analysis for the expression of ANXA2, E-cadherin, vimentin, and slug in $ISK^{control}$ cells and ISK^{ANXA2} cells. β-Actin was used as a loading control. *B*, representative phase contrast images of $ISK^{control}$ cells and ISK^{ANXA2} cells growing in monolayer cultures. *C*, double immunofluorescence localization of ANXA2, E-cadherin, vimentin, and slug in $ISK^{control}$ cells and ISK^{ANXA2} cells. The cells were stained for ANXA2, E-cadherin, vimentin, and slug, respectively, and counterstained with DAPI to visualize the nuclei. *D*, representative images of colonies formed in $ISK^{control}$ cells, ISK^{NC} cells, and ISK ^{ANXA2} cells, respectively. *E*, ISK^{NC} cells, ISK^{ANXA} cells, and ISK cells treated with LiCl were subjected to TOP/FOP flash assay. ISK cells treated with LiCl were considered as positive control. *F*, relative mRNA levels of the four established β-catenin target genes including c-Myc, cyclin D1, c-Jun, and MMP-7 were quantified in $ISK^{control}$ cells, ISK^{ANXA2} cells, and ISK cells treated with LiCl as normalized to the mRNA levels of GAPDH. All of the data are from at least three independent experiments and are shown as the means ± S.D. *, $p < 0.05$; **, $p < 0.01$; ***, $p < 0.001$; *ns*, not significant.

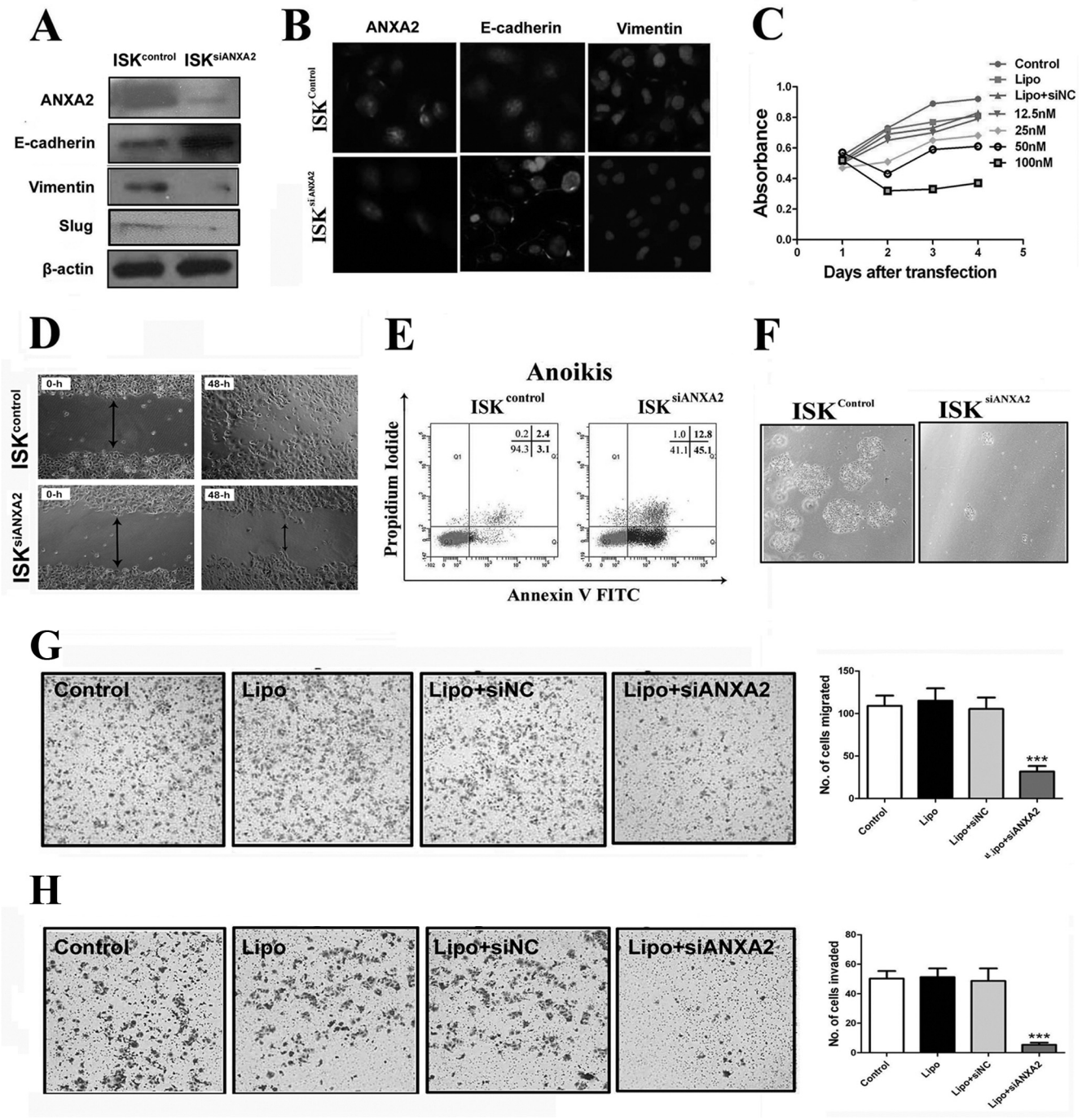

FIG. 5. **Effects of siRNA-based inhibition of ANXA2 expression on proliferation, migration, invasion, and anchorage-independent growth of ISK cells.** *A*, immunoblotting analysis of $ISK^{siANXA2}$ cells and $ISK^{control}$ cells for ANXA2, E-cadherin, vimentin, and slug was performed using whole cell lysates. *β*-Actin was used as a loading control. *B*, immunofluorescence localization of ANXA2, E-cadherin, and vimentin in $ISK^{control}$ cells and $ISK^{siANXA2}$ cells. The cells were stained for ANXA2, E-cadherin, and vimentin, respectively, and counterstained with DAPI to visualize the nuclei. *C*, cellular proliferation was measured in $ISK^{control}$, ISK^{lipo}, ISK^{siNC}, and $ISK^{siANXA2}$ cells using MTT assay. *D*, representative photomicrographs of cell migration by monolayer wound healing assay using $ISK^{control}$ cells and $ISK^{siANXA2}$ cells. Photomicrographs were obtained 0 and 48 h after standard scrape wounding. *E*, the anoikis assay was performed by plating the $ISK^{control}$ and $ISK^{siANXA2}$ cells on polyHEMA-coated culture dishes for 72 h. *F*, representative images of viable cells after anoikis challenge. *G*, cell migration assay was performed using 24-well Transwell plates after 24 h of plating. *H*, cell invasion assay was performed using 24-well Transwell plates coated with the Matrigel after 48 h of plating. All of the data are from at least three independent experiments and are shown as the means ± S.D. *, $p < 0.05$; **, $p < 0.01$; ***, $p < 0.001$.

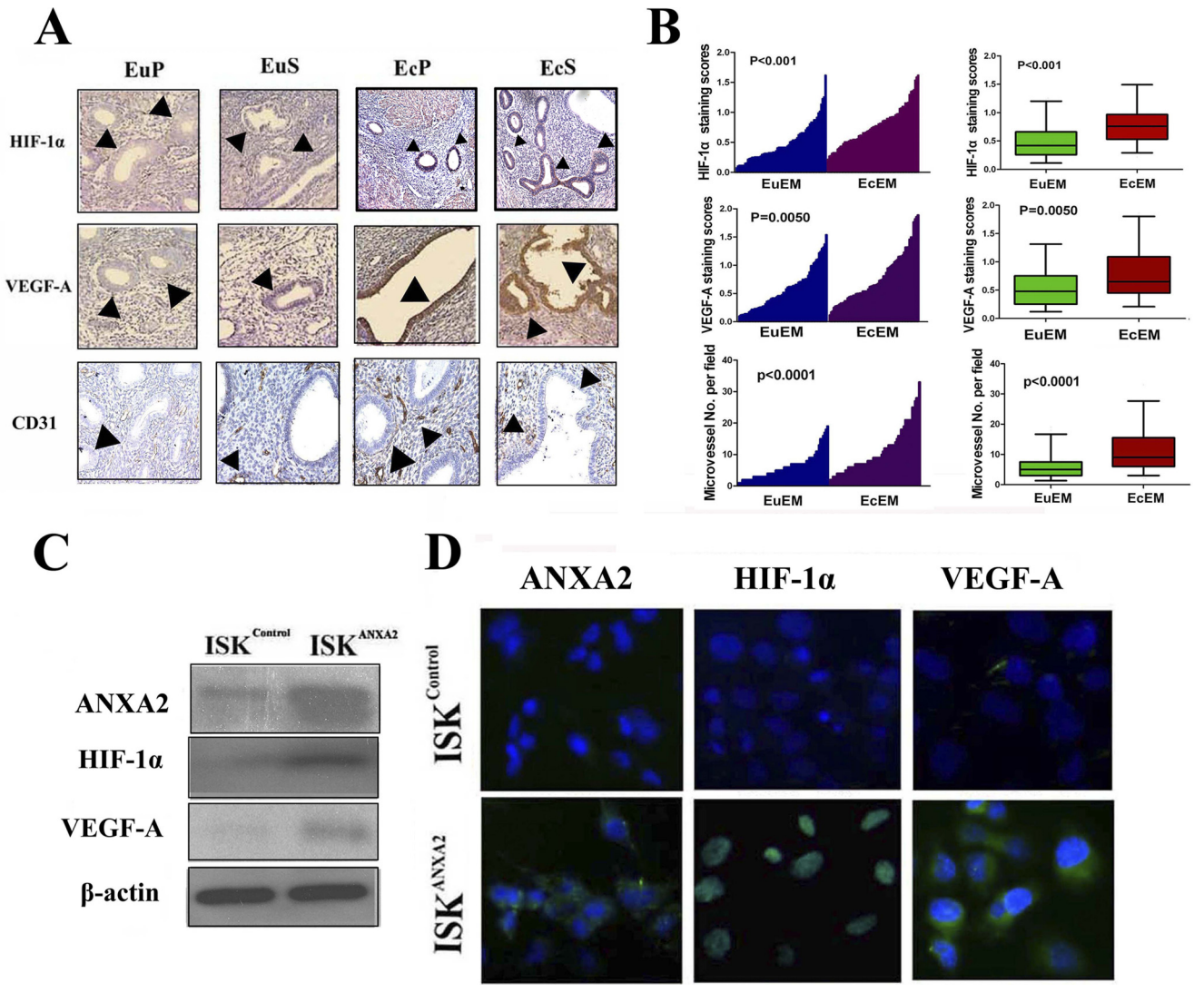

FIG. 6. **ANXA2 overexpression in ectopic endometrium is correlated with HIF-1α/VEGF-A signaling pathway activation in adenomyosis.** *A*, matched eutopic and ectopic endometrial tissues either in proliferative phase (*EuP* and *EcP*) or secretory phase (*EuS* and *EcS*) were analyzed for HIF-1α, VEGF-A, and CD31 by immunohistochemistry. *B*, HIF-1α, VEGF-A, and CD31 expression in matched eutopic and ectopic endometrium of adenomyosis were plotted using the IHC staining scores ($n = 65$). *C*, immunoblotting analysis of ISK^{ANXA2} cells and $ISK^{control}$ cells for ANXA2, HIF-1α, and VEGF-A using whole cell lysates. β-Actin was used as a loading control. *D*, immunofluorescence localization of ANXA2, HIF-1α, and VEGF-A in $ISK^{control}$ cells and ISK^{ANXA2} cells. The cells were stained for ANXA2, HIF-1α, and VEGF-A, respectively, and counterstained with DAPI to visualize the nuclei.

neurogenic phase that is directly stimulated in the paw with the release of substance P. The late phase refers to the inflammation pain response involving the release of histamine, serotonin, bradykinin, and prostaglandin. As shown in Fig. 8*I*, ANXA2 knockdown revealed significant analgesic effects on formalin-induced pain in both early (0–5 min) and late phases (15–30 min). These observations implied that ANXA2 inhibition could alleviate adenomyosis-induced hyperalgesia in nude mice, which might serve as a potential therapeutic strategy to alleviate dysmenorrhea in adenomyosis patients.

Further immunohistochemistry analysis revealed remarkable EMT marker alterations, including decreased vimentin and increased E-cadherin expression in the implanted adenomyotic tissues of nude mice treated with Lipo-ANXA2 shRNA compared with NS, Lipo, or Lipo-NC shRNA-treated counterparts (Fig. 9). Moreover, HIF-1α/VEGF-A pathway was also abrogated in the implanted endometrial tissue of Lipo-ANXA2 shRNA-treated nude mice (Fig. 9). Accordingly, the microvessel densities in the implanted endometrial tissues of nude mice treated with Lipo-ANXA2 shRNA were significantly lower than those in the control groups (Fig. 9). Xenotransplanted adenomyotic lesions were also evaluated for markers of proliferation (Ki67) and apoptosis (TUNEL assay). Increased apoptosis and decreased proliferation were observed in grafted adenomyotic lesions treated with

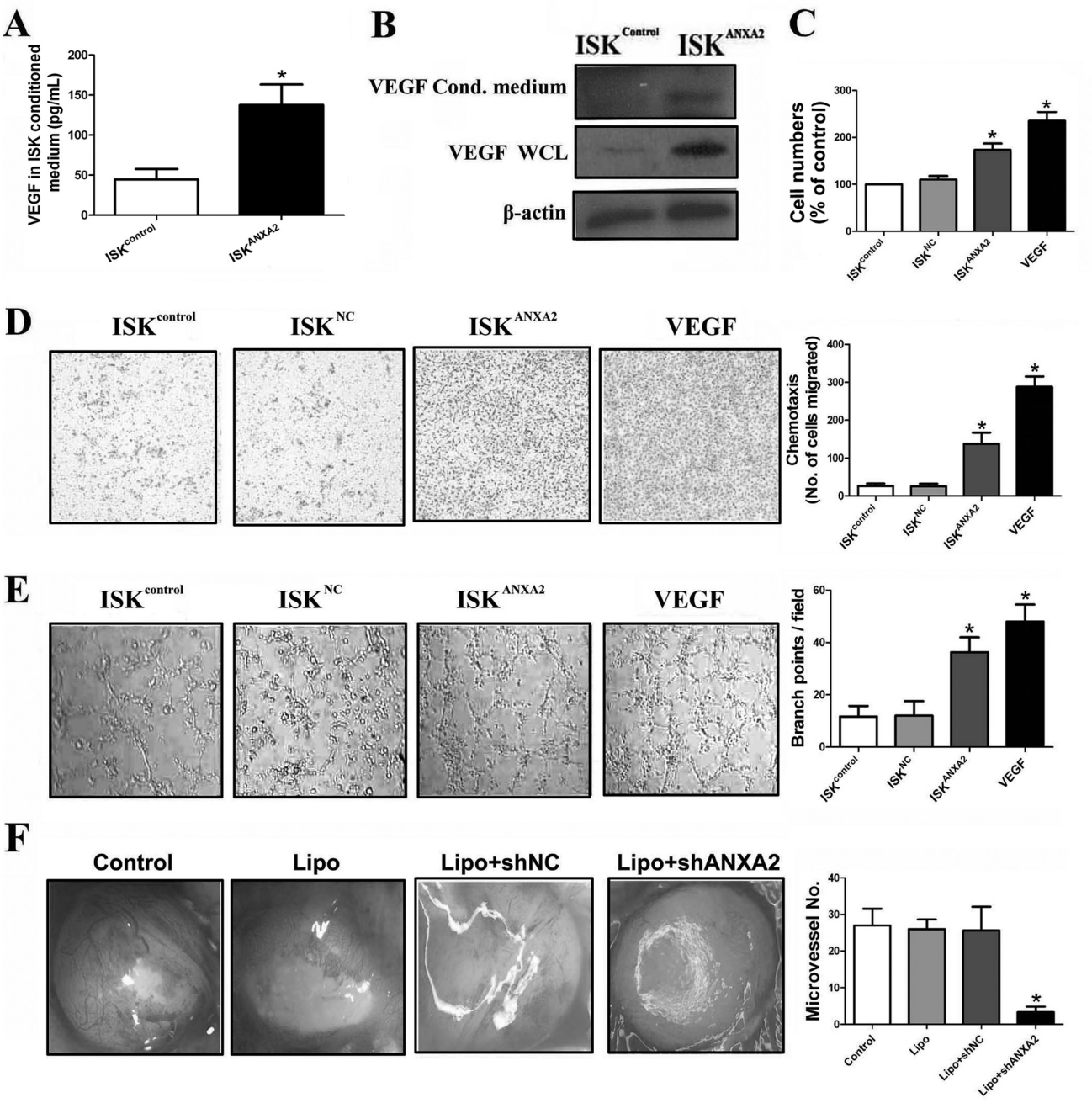

FIG. 7. **ANXA2 modulates proangiogenesis of adenomyotic endometrial cells both *in vitro* and *in vivo*.** *A*, ELISA analysis of VEGF in the conditioned media of $ISK^{control}$ cells and ISK^{ANXA2} cells. *B*, immunoblotting analysis of VEGF in both conditioned (*Cond.*) media and whole cell lysates of $ISK^{control}$ cells and ISK^{ANXA2} cells. β-Actin was used as a loading control. *C*, the conditioned media of ISK cells on the proliferation of HUVEC cells by MTT assay. HUVEC cells were cultured by either $ISK^{control}$-, ISK^{NC}-, or ISK^{ANXA2}-conditioned media. Medium with the addition of VEGF was used as positive control. *D*, the conditioned media of ISK cells on the motility of HUVEC cells. HUVEC cells were cultured by either $ISK^{control}$-, ISK^{NC}-, or ISK^{ANXA2}-conditioned media, and the motility of HUVEC cells was performed using 24-well Transwell plates. Medium with the addition of VEGF was used as positive control. *E*, tube formation of either $ISK^{control}$-, ISK^{NC}-, or ISK^{ANXA2}-conditioned medium-treated HUVECs on Matrigel. Medium with the addition of VEGF was used as positive control. *F*, representative pictures of new blood vessels on alginate beads in NS-, Lipo-, Lipo + shNC-, or Lipo + shANXA2-treated nude mice. All of the data are from at least three independent experiments and are shown as the means ± S.D. *, $p < 0.05$; **, $p < 0.01$; ***, $p < 0.001$.

Lipo-ANXA2 shRNA, compared with those in the control groups (Fig. 9). These observations proved that ANXA2 knockdown attenuated xenotransplanted adenomyotic lesion growth, metastasis, and angiogenesis in nude mice via reverting EMT process and inhibiting HIF-1α/VEGF-A pathway activation.

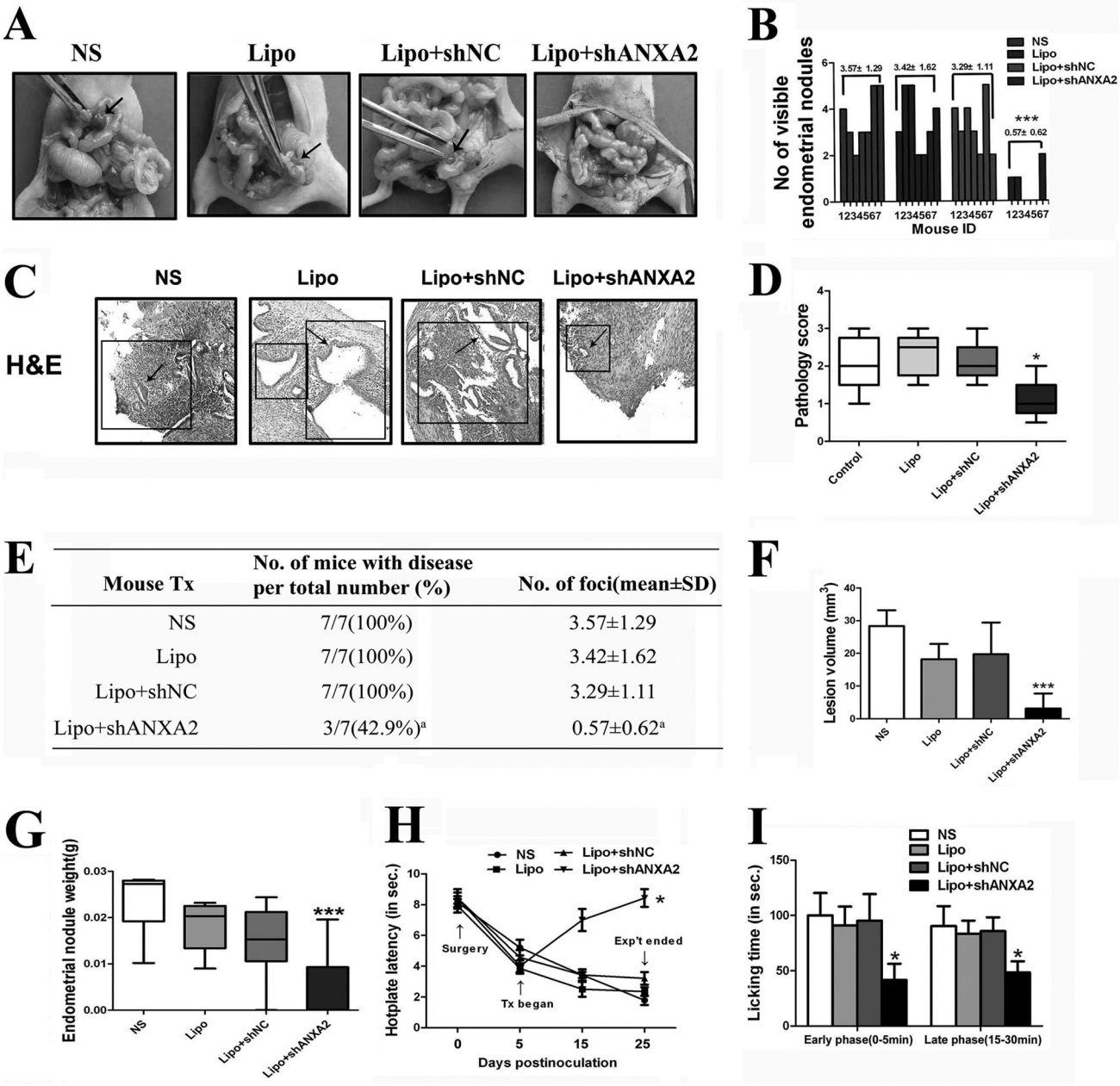

Mouse Tx	No. of mice with disease per total number (%)	No. of foci(mean±SD)
NS	7/7(100%)	3.57±1.29
Lipo	7/7(100%)	3.42±1.62
Lipo+shNC	7/7(100%)	3.29±1.11
Lipo+shANXA2	3/7(42.9%)[a]	0.57±0.62[a]

FIG. 8. **Effects of inhibition of ANXA2 expression on experimental adenomyosis model in nude mice.** *A*, representative images of NS-, Lipo-, Lipo + shNC-, or Lipo+shANXA2-treated adenomyosis nude mice model. The *black arrows* indicate adenomyotic lesion sites. *B*, the number of endometrial nodules was quantified in adenomyosis nude mice model in each group ($n = 7$ per group). *C*, representative images of serial haematoxylin and eosin (*H&E*) staining of adenomyosis lesion sections. *D*, pathology scores of experimental adenomyosis in nude mice of each group. *E*, summary of the incidence of adenomyotic nodules in NS-, Lipo-, Lipo + shNC-, or Lipo + shANXA2-treated adenomyosis nude mice model at the time of sacrifice ($n = 7$ per group). [a] indicates $p < 0.05$. *F*, the lesion volume of endometrial nodules was measured in adenomyosis nude mice model in each group 25 days postinoculation ($n = 7$ per group). *G*, the weight of endometrial nodules was quantified in adenomyosis nude mice model in each group 25 days postinoculation ($n = 7$ per group). *H*, time course of changes in average hot plate latency in respective groups. The abbreviated words in the figure represent different time points: *Tx* stands for treatment, and *Exp't* stands for experiment. *I*, effects of the ANXA2 knockdown on formalin-induced pain in the hindpaw of adenomyosis nude mice model. Paw licking time was measured in early phase (0–5 min) and late phase (15–30 min), respectively. All of the data are from at least three independent experiments and are shown as the means ± S.D. *, $p < 0.05$; **, $p < 0.01$; ***, $p < 0.001$.

DISCUSSION

Adenomyosis development mimics the process of tumor metastasis, which is characterized by progressive *trans*-myometrial invasion of endometrial cells and neovascularization in ectopic lesions. Emerging evidence suggests that the process of adenomyosis development is closely associated with ele-

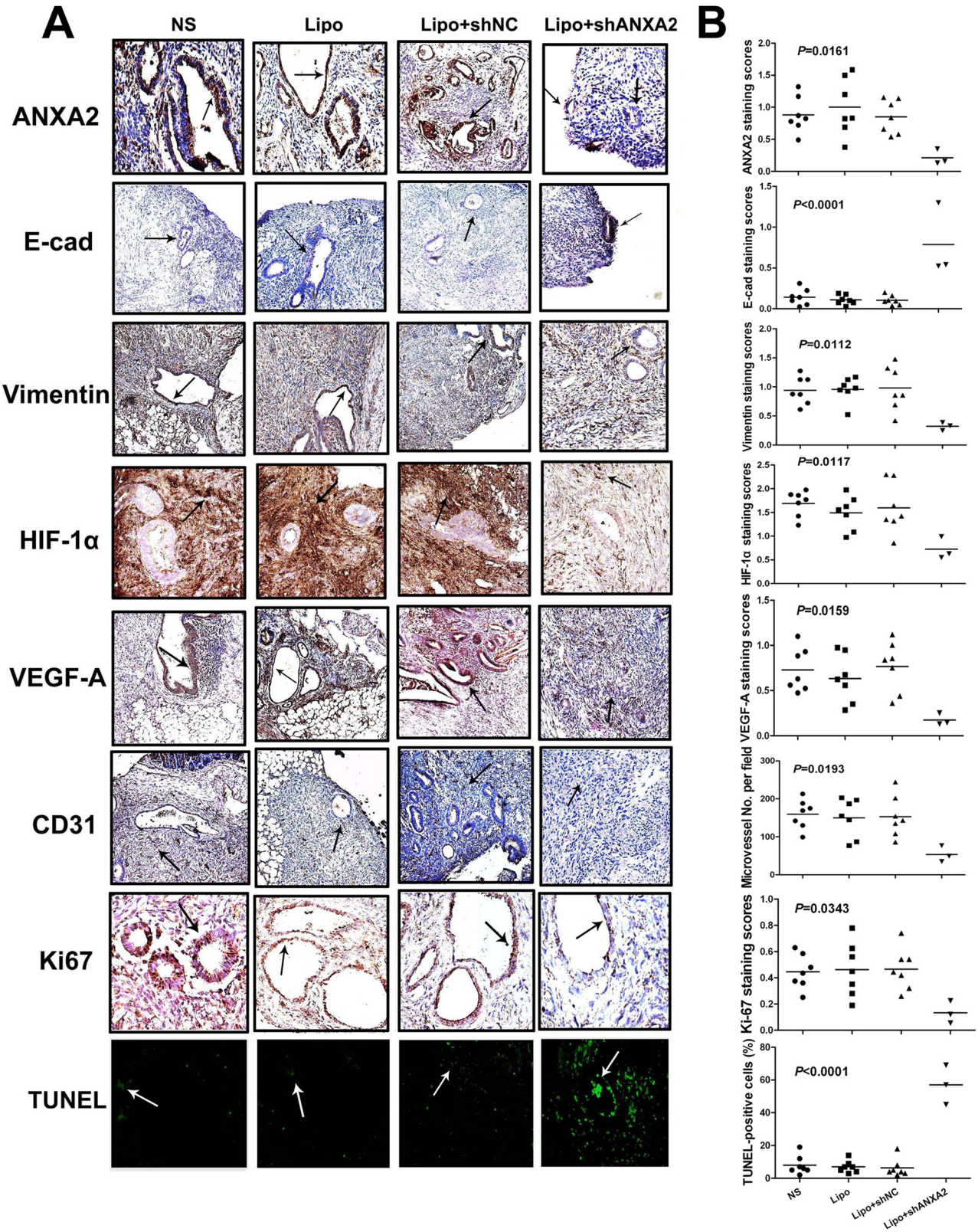

FIG. 9. **Knockdown of ANXA2 decreases proliferation, metastatic potential and proangiogenesis capacity of adenomyotic endometrial cells *in vivo*.** *A*, specimens of experimental adenomyosis model of nude mice in each group were immunostained for ANXA2, E-cadherin (*E-cad*), vimentin, HIF-1α, VEGF-A, CD31, Ki-67, and TUNEL assay. *B*, scatter plot of expression level of each indicated molecule in the experimental adenomyosis nude mice model in each group (n = 7 per group).

vated serum E2 concentration (1). However, the molecular events underlying its pathogenesis remain underexplored. Herein, we utilized 2-DE-based proteomics analysis to compare the differential protein expression profile between matched ectopic and eutopic endometrium of adenomyosis and identified a group of estrogen-responsive proteins as significantly altered. Among them, ANXA2 was proved to constitute a key player in adenomyosis development by inducing both metastasis and proangiogenesis of adenomyotic endometrial cells.

The presenting symptoms of adenomyosis encompass a soft and diffusely enlarged uterus, dysmenorrhea, abnormal uterine bleeding, and subfertility, with dysmenorrhea being the second most prevalent symptom after abnormal uterine bleeding and possibly the most debilitating. Treatment of adenomyosis has been a challenge, with hysterectomy being the treatment of choice for severe and symptomatic adenomyosis (2). Hitherto, the molecular mechanisms underlying adenomyosis-associated dysmenorrhea are poorly understood. Previous studies reported that decreased immunoreactivity to progesterone receptor isoform B and increased immunoreactivity to nuclear factor κB, oxytocin receptor, SLIT/ROBO1, and transient receptor potential vanilloid type 1 were tightly correlated with the severity of dysmenorrhea in adenomyosis patients. These molecules are either directly or indirectly linked to inflammation and other pain mediators (20, 30). Interestingly, our 2-DE/MS analysis-derived data identified ANXA2 as a key factor in adenomyosis development, whose expression level in ectopic lesion was proved positively correlated with severity of adenomyosis-associated dysmenorrhea. Moreover, ANXA2 knockdown in adenomyosis nude mice model could significantly alleviate generalized hyperalgesia, which was considered to be a concomitant symptom with dysmenorrhea in adenomyosis (20). Therefore, ANXA2 might serve as a potential noninvasive target for the treatment of adenomyosis-induced dysmenorrhea.

In this study, we also found that E2, as a ubiquitous ligand for both estrogen receptors α and β, could mediate the switch of endometrial cells to a mesenchymal phenotype. Dysregulated E2 metabolism has been reported to contribute to a variety of human diseases including leiomyoma, endometriosis, osteoporosis, Parkinson disease, and gynecological malignancies (31–35). Recently, Flamini *et al.* (36) reported that E2 could regulate endometrial cell cytoskeletal remodeling and motility via focal adhesion kinase. Our study proved that ANXA2, identified by our proteomics analysis, served as a downstream target of E2. E2-induced up-regulation of ANXA2 was correlated with down-regulation of E-cadherin and enhanced expression of vimentin and slug in adenomyotic endometrial cells, thus facilitating them to undergo EMT-switch and acquire increased migratory potential. These data provide molecular evidence to support the notion that E2 plays a critical role in adenomyosis development.

Annexin family proteins have been reported to participate in a variety of cellular processes including endocytosis, exocytosis, and cellular adhesion (37). As a member of annexin family proteins, ANXA2 could bind to certain membrane phospholipids in a Ca^{2+}-dependent manner, providing a link between Ca^{2+} signaling and membrane functions. By forming networks on the membrane surface, ANXA2 serves as an organizer of membrane domains and membrane recruitment platforms for proteins with which they interact (38). Recently, one group reported that ANXA2 constitutes a critical node in triggering Rho/ROCK-dependent and actin-mediated changes in cell morphology associated with the control of cell adhesion (39). ANXA2 inhibition also revealed its role in regulating several cellular processes that range from membrane dynamics to cell differentiation and migration. Additionally, ANXA2 functions as one of the receptors for plasminogen and tPA, which binds to plasminogen and converts it to plasmin. Because the proteolytic capacity of plasmin is intricately regulated, uncontrolled generation of plasmin can degrade extracellular matrix and basement membrane of the surrounding blood vessels (40). Hence, ANXA2-dependent plasmin generation contributes to neoangiogenesis and cancer progression. In this study, we proved that ANXA2 overexpression was tightly correlated with metastatic potential as well as proangiogenesis capacity of adenomyotic endometrial cells via initiation of EMT phenotype and activation of HIF-1α/VEGFA signaling pathway, respectively.

EMT involves dedifferentiation of polarized epithelial cells to a migratory fibroblastoid phenotype, a phenomenon that is increasingly considered to be an important event during cancer progression and metastasis (3). It is accompanied by a profoundly altered mesenchymal gene expression program, which is characterized by loss of epithelial keratins like E-cadherin and induction of mesenchymal vimentin (41). EMT could be categorized into three subtypes based upon respective biologic effects (5). Type 1 EMT occurs during embryonic development. Type 2 EMT is responsible for wound healing, tissue regeneration, and organ fibrosis. Type 3 EMT occurs during metastatic progression. Of all the three types of EMT, induction of vimentin is an important early event in the pathway toward EMT, and the hallmark of EMT is the loss of expression of the cell adhesion molecule E-cadherin (5). E-cadherin is a cell-cell adhesion molecule that participates in homotypic, calcium-dependent interactions to form epithelial adherens junctions. This function is critical in the development and maintenance of a polar epithelium. Hitherto, the functional role of ANXA2 in EMT process remains elusive. Our study demonstrated that ANXA2 overexpression was positively associated with EMT in adenomyotic endometrial cells. Enforced expression of ANXA2 in ISK cells resulted in EMT-like protein expression profile shift via β-catenin/Tcf signaling activation, and inhibition of ANXA2 led to reversal of their migratory phenotype and anoikis resistance. ANXA2 knockdown in adenomyosis nude mice model demonstrated rever-

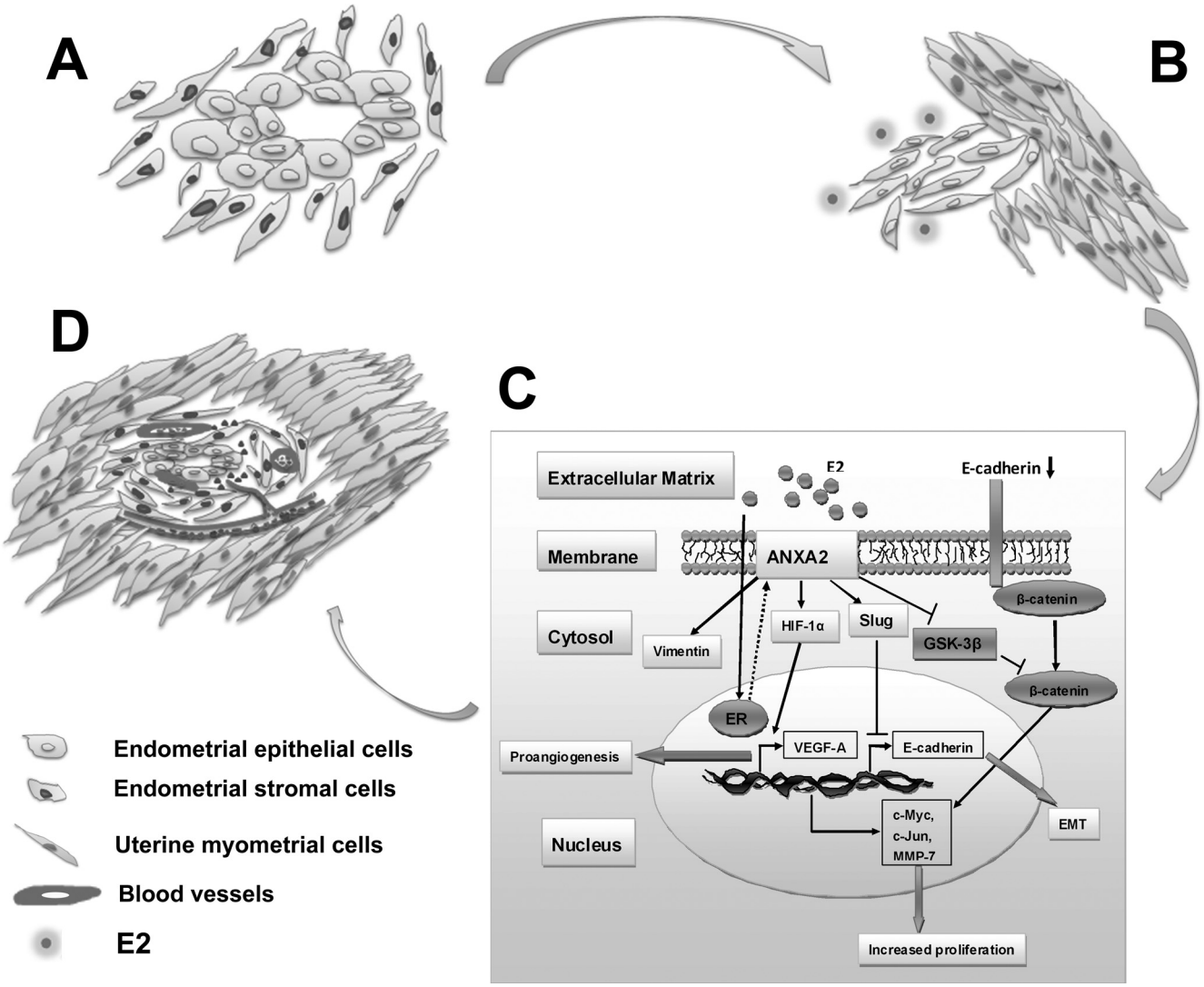

FIG. 10. **A schematic model for the role of ANXA2 in the pathogenesis of adenomyosis.** *A*, uterine endometrium under normal conditions. *B*, under elevated E2 concentration, endometrial epithelial cells undergo EMT process and acquire increased migration potential. *C*, molecular events during E2-induced EMT in adenomyosis development. Increased E2 level in females might lead to overexpression of ANXA2 in endometrial epithelial cells that causes EMT. This process involves E-cadherin suppression and vimentin induction in ANXA2-overexpressing cells. Loss of E-cadherin expression, together with inhibition of GSK-3β, results in nuclear localization of β-catenin that activates β-catenin/Tcf signaling. Hence, these cells may acquire increased capacity of proliferation, motility, invasion, and anoikis resistance in the new microenvironment. Moreover, ANXA2-expressing cells could activate the HIF-1α/VEGF-A signaling pathway that contributes to neovascularization in the new microenvironment that supports the ectopic growth of endometrium during the pathogenesis of adenomyosis. *D*, ectopic growth of endometrium supported by neovasculature in adenomyosis.

sion of mesenchymal phenotype to epithelial phenotype of adenomyotic tissues and blunted implanted endometrial tissue growth. Hence, our study demonstrated that ANXA2 overexpression could induce β-catenin/Tcf-associated EMT phenotype in adenomyotic endometrial cells.

Abnormal angiogenesis constitutes one of the key hallmarks of cancer and ischemic and inflammatory diseases and is responsible for disease progression. The angiogenic capacity is partially mediated by the hypoxia-inducible factor (HIF) family of transcription factors, which are critical regulators of oxygen homeostasis and are composed of an oxygen-labile α subunit and a constitutive β subunit (8). Given the multiple roles of HIF in tumor progression, mutations that enhance HIF activity have been thought to participate in a variety of human malignancies. However, no genetic mutations in any of the HIF subunits affecting the stability or activity of these proteins have been identified in human tumors so far. In this context, elevated HIF levels in cancers might stem from mutations of key regulators of HIF stability. Mutation of the von Hippel-Lindau gene, an upstream negative regulator of HIF, accounts for a subset of tumors with elevated HIF levels. Stabilized HIF transfers into the nucleus through binding to the Hsp90-p300/

CBP complex and subsequently activates expression of its target genes, which include VEGF-A (42). VEGF-A functions in a wide spectrum of angiogenesis processes. Activated HIF-1α/VEGF-A signaling pathway has been proved positively correlated with the growth of solid tumors, and its activation in a wide variety of tumor types signifies poor prognosis, resistance to radiotherapy and chemotherapy, and increased patient mortality (43, 44). Neovascularization has been reported in ectopic endometrium of adenomyosis (10). Our results provided additional support to this conclusion by proving that microvessel density was significantly higher in ectopic endometrium of adenomyosis compared with its eutopic counterpart. Moreover, we demonstrated that this enhanced neovascularization resulted from ANXA2-dependent HIF-1α/VEGFA activation. Hence, our study suggested that ANXA2 overexpression contributes to neovascularization of adenomyotic lesion in a HIF-1α/VEGFA-dependent manner.

In conclusion, our study identified ANXA2 as one of the key contributors to the pathogenesis of adenomyosis using a 2-DE-based proteomics approach. We further proved that the expression of ANXA2 could be up-regulated under elevated level of E2 concentration. The invasive and metastatic potential involved in adenomyosis was achieved by ANXA2-induced β-catenin/Tcf-associated EMT-like switch in endometrial cells and the proangiogenic capacity in local lesion was enhanced via ANXA2/HIF-1α/VEGF-A pathway activation (Fig. 10). Moreover, the expression levels of ANXA2 in ectopic lesion were tightly correlated with dysmenorrhea severity in adenomyosis patients. Its inhibition could effectively attenuate adenomyosis-induced hyperalgesia in nude mice. Hence, the critical role of ANXA2 in adenomyosis pathogenesis renders it a novel therapeutic target for the treatment of adenomyosis in future clinical practice.

* This work was supported by National Basic Research Program of China Grants 2010CB529905 and 2011CB910703, National Key Technologies R&D Program Grant 2012ZX09501001-003, and National Natural Science Foundation of China Grants 81072022 and 81172173.

‡ To whom correspondence may be addressed. Tel.: 86-28-85501633; Fax: 86-28-85164046; E-mail: xia-zhao@126.com.

§ To whom correspondence may be addressed. Tel.: 86-13258370346; Fax: 86-28-85164060; E-mail: hcanhua@hotmail.com.

REFERENCES

1. Ferenczy, A. (1998) Pathophysiology of adenomyosis. *Hum. Reprod. Update* **4,** 312–322
2. Bergholt, T., Eriksen, L., Berendt, N., Jacobsen, M., and Hertz, J. B. (2001) Prevalence and risk factors of adenomyosis at hysterectomy. *Hum. Reprod.* **16,** 2418–2421
3. Williams, C. S., Zhang, B., Smith, J. J., Jayagopal, A., Barrett, C. W., Pino, C., Russ, P., Presley, S. H., Peng, D., Rosenblatt, D. O., Haselton, F. R., Yang, J. L., Washington, M. K., Chen, X., Eschrich, S., Yeatman, T. J., El-Rifai, W., Beauchamp, R. D., and Chang, M. S. (2011) BVES regulates EMT in human corneal and colon cancer cells and is silenced via promoter methylation in human colorectal carcinoma. *J. Clin. Invest.* **121,** 4056–4069
4. Terao, M., Ishikawa, A., Nakahara, S., Kimura, A., Kato, A., Moriwaki, K., Kamada, Y., Murota, H., Taniguchi, N., Katayama, I., and Miyoshi, E. (2011) Enhanced epithelial-mesenchymal transition-like phenotype in N-acetylglucosaminyltransferase V transgenic mouse skin promotes wound healing. *J. Biol. Chem.* **286,** 28303–28311
5. Cannito, S., Novo, E., di Bonzo, L. V., Busletta, C., Colombatto, S., and Parola, M. (2010) Epithelial-mesenchymal transition: From molecular mechanisms, redox regulation to implications in human health and disease. *Antioxid. Redox. Signal.* **12,** 1383–1430
6. Scotti, S., Regidor, P. A., Schindler, A. E., and Winterhager, E. (2000) Reduced proliferation and cell adhesion in endometriosis. *Mol. Hum. Reprod.* **6,** 610–617
7. Zhang, H., Niu, Y., Feng, J., Guo, H., Ye, X., and Cui, H. (2006) Use of proteomic analysis of endometriosis to identify different protein expression in patients with endometriosis versus normal controls. *Fertil. Steril.* **86,** 274–282
8. Potente, M., Gerhardt, H., and Carmeliet, P. (2011) Basic and therapeutic aspects of angiogenesis. *Cell* **146,** 873–887
9. Koh, Y. J., Kim, H. Z., Hwang, S. I., Lee, J. E., Oh, N., Jung, K., Kim, M., Kim, K. E., Kim, H., Lim, N. K., Jeon, C. J., Lee, G. M., Jeon, B. H., Nam, D. H., Sung, H. K., Nagy, A., Yoo, O. J., and Koh, G. Y. (2010) Double antiangiogenic protein, DAAP, targeting VEGF-A and angiopoietins in tumor angiogenesis, metastasis, and vascular leakage. *Cancer Cell* **18,** 171–184
10. Ota, H., Igarashi, S., and Tanaka, T. (1998) Morphometric evaluation of stromal vascularization in the endometrium in adenomyosis. *Hum. Reprod.* **13,** 715–719
11. Li, Z., Zhao, X., Bai, S., Wang, Z., Chen, L., Wei, Y., and Huang, C. (2008) Proteomics identification of cyclophilin A as a potential prognostic factor and therapeutic target in endometrial carcinoma. *Mol. Cell. Proteomics* **7,** 1810–1823
12. Liu, R., Li, Z., Bai, S., Zhang, H., Tang, M., Lei, Y., Chen, L., Liang, S., Zhao, Y. L., Wei, Y., and Huang, C. (2009) Mechanism of cancer cell adaptation to metabolic stress: Proteomics identification of a novel thyroid hormone-mediated gastric carcinogenic signaling pathway. *Mol. Cell. Proteomics* **8,** 70–85
13. Jensen, L. J., Kuhn, M., Stark, M., Chaffron, S., Creevey, C., Muller, J., Doerks, T., Julien, P., Roth, A., Simonovic, M., Bork, P., and von Mering, C. (2009) STRING 8: A global view on proteins and their functional interactions in 630 organisms. *Nucleic Acids Res.* **37,** D412–D416
14. Zhang, S., Cao, Z., Tian, H., Shen, G., Ma, Y., Xie, H., Liu, Y., Zhao, C., Deng, S., Yang, Y., Zheng, R., Li, W., Zhang, N., Liu, S., Wang, W., Dai, L., Shi, S., Cheng, L., Pan, Y., Feng, S., Zhao, X., Deng, H., Yang, S., and Wei, Y. (2011) SKLB1002, a novel potent inhibitor of VEGF receptor 2 signaling, inhibits angiogenesis and tumor growth *in vivo. Clin. Cancer Res.* **17,** 4439–4450
15. Bai, Y., Deng, H., Yang, Y., Zhao, X., Wei, Y., Xie, G., Li, Z., Chen, X., Chen, L., Wang, Y., Su, D., Qian, Z., Zhong, Q., Luo, H., and Yi, T. (2009) VEGF-targeted short hairpin RNA inhibits intraperitoneal ovarian cancer growth in nude mice. *Oncology* **77,** 385–394
16. Ryzhova, E. V., Vos, R. M., Albright, A. V., Harrist, A. V., Harvey, T., and González-Scarano, F. (2006) Annexin 2: A novel human immunodeficiency virus type 1 Gag binding protein involved in replication in monocyte-derived macrophages. *J. Virol.* **80,** 2694–2704
17. Chen, Y. J., Li, H. Y., Huang, C. H., Twu, N. F., Yen, M. S., Wang, P. H., Chou, T. Y., Liu, Y. N., Chao, K. C., and Yang, M. H. (2010) Oestrogen-induced epithelial-mesenchymal transition of endometrial epithelial cells contributes to the development of adenomyosis. *J. Pathol.* **222,** 261–270
18. Ngô, C., Nicco, C., Leconte, M., Chéreau, C., Arkwright, S., Vacher-Lavenu, M. C., Weill, B., Chapron, C., and Batteux, F. (2010) Protein kinase inhibitors can control the progression of endometriosis *in vitro* and *in vivo. J. Pathol.* **222,** 148–157
19. Nie, J., Liu, X., and Guo, S. W. (2010) Immunoreactivity of oxytocin receptor and transient receptor potential vanilloid type 1 and its correlation with dysmenorrhea in adenomyosis. *Am. J. Obst. Gynecol.* **202,** 346.e1–346.e8
20. Lu, Y., Nie, J., Liu, X., Zheng, Y., and Guo, S. W. (2010) Trichostatin A, a histone deacetylase inhibitor, reduces lesion growth and hyperalgesia in experimentally induced endometriosis in mice. *Hum. Reprod.* **25,** 1014–1025
21. Dang, Y. H., Xing, B., Zhao, Y., Zhao, X. J., Huo, F. Q., Tang, J. S., Qu, C. L., and Chen, T. (2011) The role of dopamine receptors in ventrolateral orbital cortex-evoked antinociception in a rat formalin test model. *Eur. J. Pharmacol.* **657,** 97–103

22. Won, K. J., Lee, P., Jung, S. H., Jiang, X., Lee, C. K., Lin, H. Y., Kang, H., Lee, H. M., Kim, J., Toyokuni, S., and Kim, B. (2011) 3-Morpholinosydnonimine participates in the attenuation of neointima formation via inhibition of annexin A2-mediated vascular smooth muscle cell migration. *Proteomics* **11,** 193–201
23. Lokman, N. A., Ween, M. P., Oehler, M. K., and Ricciardelli, C. (2011) The role of annexin A2 in tumorigenesis and cancer progression. *Cancer Microenviron.* **4,** 199–208
24. Eyster, K. M., Klinkova, O., Kennedy, V., and Hansen, K. A. (2007) Whole genome deoxyribonucleic acid microarray analysis of gene expression in ectopic versus eutopic endometrium. *Fertil. Steril.* **88,** 1505–1533
25. Hever, A., Roth, R. B., Hevezi, P., Marin, M. E., Acosta, J. A., Acosta, H., Rojas, J., Herrera, R., Grigoriadis, D., White, E., Conlon, P. J., Maki, R. A., and Zlotnik, A. (2007) Human endometriosis is associated with plasma cells and overexpression of B lymphocyte stimulator. *Proc. Natl. Acad. Sci. U.S.A.* **104,** 12451–12456
26. Burney, R. O., Talbi, S., Hamilton, A. E., Vo, K. C., Nyegaard, M., Nezhat, C. R., Lessey, B. A., and Giudice, L. C. (2007) Gene expression analysis of endometrium reveals progesterone resistance and candidate susceptibility genes in women with endometriosis. *Endocrinology* **148,** 3814–3826
27. Tsuji, T., Ibaragi, S., and Hu, G. F. (2009) Epithelial-mesenchymal transition and cell cooperativity in metastasis. *Cancer Res.* **69,** 7135–7139
28. Dhawan, P., Singh, A. B., Deane, N. G., No, Y., Shiou, S. R., Schmidt, C., Neff, J., Washington, M. K., and Beauchamp, R. D. (2005) Claudin-1 regulates cellular transformation and metastatic behavior in colon cancer. *J. Clin. Invest.* **115,** 1765–1776
29. Sood, A.K, Armaiz-Pena, G. N., Halder, J., Nick, A. M., Stone, R. L., Hu, W., Carroll, A. R., Spannuth, W. A., Deavers, M. T., Allen, J. K., Han, L. Y., Kamat, A. A., Shahzad, M. M., McIntyre, B. W., Diaz-Montero, C. M., Jennings, N. B., Lin, Y. G., Merritt, W. M., DeGeest, K., Vivas-Mejia, P. E., Lopez-Berestein, G., Schaller, M. D., Cole, S. W., and Lutgendorf, S. K. (2010) Adrenergic modulation of focal adhesion kinase protects human ovarian cancer cells from anoikis. *J. Clin. Invest.* **120,** 1515–1523
30. Liu, X., and Guo, S. W. (2011) Valproic acid alleviates generalized hyperalgesia in mice with induced adenomyosis. *J. Obst. Gynaecol. Res.* **37,** 696–708
31. Al-Hendy, A., and Salama, S. (2006) Gene therapy and uterine leiomyoma: A review. *Hum. Reprod. Update* **12,** 385–400
32. Bulun, S. E., Monsavais, D., Pavone, M. E., Dyson, M., Xue, Q., Attar, E., Tokunaga, H., and Su, E. J. (2012) Role of estrogen receptor-β in endometriosis. *Semin. Reprod. Med.* **30,** 39–45
33. Lecart, M. P., and Reginster, J. Y. (2011) Current options for the management of postmenopausal osteoporosis. *Expert Opin. Pharmacother.* **12,** 2533–2552
34. Morissette, M., Al Sweidi, S., Callier, S., and Di Paolo, T. (2008) Estrogen and SERM neuroprotection in animal models of Parkinson's disease. *Mol. Cell. Endocrinol.* **290,** 60–69
35. Lam, E. W., Shah, K., and Brosens, J. J. (2012) The diversity of sex steroid action: The role of micro-RNAs and FOXO transcription factors in cycling endometrium and cancer. *J. Endocrinol.* **212,** 13–25
36. Flamini, M. I., Sanchez, A. M., Genazzani, A. R., and Simoncini, T. (2011) Estrogen regulates endometrial cell cytoskeletal remodeling and motility via focal adhesion kinase. *Fertil. Steril.* **95,** 722–726
37. Mussunoor, S., and Murray, G. I. (2008) The role of annexins in tumour development and progression. *J. Pathol.* **216,** 131–140
38. Sharma, M. C., and Sharma, M. (2007) The role of annexin II in angiogenesis and tumor progression: A potential therapeutic target. *Curr. Pharm. Des.* **13,** 3568–3575
39. Rescher, U., Ludwig, C., Konietzko, V., Kharitonenkov, A., and Gerke, V. (2008) Tyrosine phosphorylation of annexin A2 regulates Rho-mediated actin rearrangement and cell adhesion. *J. Cell Sci.* **121,** 2177–2185
40. Valapala, M., Thamake, S. I., and Vishwanatha, J. K. (2011) A competitive hexapeptide inhibitor of annexin A2 prevents hypoxia-induced angiogenic events. *J. Cell Sci.* **124,** 1453–1464
41. Weber, G. F., Bjerke, M. A., and DeSimone, D. W. (2011) Integrins and cadherins join forces to form adhesive networks. *J. Cell Sci.* **124,** 1183–1193
42. Semenza, G. L. (2003) Targeting HIF-1 for cancer therapy. *Nat. Rev. Cancer* **3,** 721–732
43. Garcia, J. A. (2006) HIFing the brakes: Therapeutic opportunities for treatment of human malignancies. *Sci STKE* 2006, pe25
44. Blagosklonny, M. V. (2004) Antiangiogenic therapy and tumor progression. *Cancer Cell* **5,** 13–17